Albana Arreza, BSc

Validation of Embedded Beam Row for Anchor Modelling in PLAXIS 2D

MASTER´S THESIS

to achieve the university degree of

Diplom-Ingenieurin

Master's programme Civil Engineering, Geotechnics and Hydraulics

submitted to

Graz University of Technology

Supervisor

Ao.Univ.-Prof. Dipl.-Ing. Dr.techn. M.Sc.

Helmut Schweiger

Institute of Soil Mechanics, Foundation Engineering and Computational Geotechnics

Co-supervisor

Dipl.-Ing. **Simon Oberhollenzer,** BSc.

Graz, November 2018

Eidesstattliche Erklärung

Ich erkläre an Eides statt, dass ich die vorliegende Arbeit selbstständig verfasst, andere als die angegebenen Quellen/Hilfsmittel nicht benutzt, und die den benutzten Quellen wörtlich und inhaltlich entnommenen Stellen als solche kenntlich gemacht habe. Das in TUGRAZonline hochgeladene Textdokument ist mit der vorliegenden Arbeit identisch.

I declare that I have authored this thesis independently, that I have not used other than the declared sources/resources, and that I have explicitly marked all material which has been quoted either literally or by content from the used sources. The text document uploaded to TUGRAZonline is identical to the present master‘s thesis.

…… ……

Datum Unterschrift

Acknowledgements

To Prof. Schweiger, for inspiring me to choose computational geotechnics as the most challenging discipline in geotechnics and for always supporting me…

To Prof. Marte, for showing me how intuitive and creative a technical field can be and for being an example for his kind and respectful way of treating others…

To Simon, for his intensive guidance throughout this thesis…

To my parents, for teaching me the meaning of unconditional love and for showing it to me when I deserved it the least and needed the most…

To my brother Endri, for always remembering me to keep searching…

To my brother Toni, for bringing me down to earth when I get lost in dreams…

To my grandpa, for always making me feel „his favourite“…

To Jelena, for helping me find the inner strength when I fall apart…

To Gor, for being such a beautiful soul…

To the people who have touched my life, but weren´t meant to be forever, for making me feel special, loved and appreciated, for helping me grow into the person I am today…

Kurzfassung

Gebirgsanker werden hauptsächlich zur Gebirgsvergütung im Berg- und Tunnelbau eingesetzt. Diverse numerische Methoden, wie z.B. die FEM (Goodman et al., 1968), die BEM (Crotty & Wardle, 1985) bzw. die Blockmethode (Cundall, 1971) haben Modelle für Felsbolzen implementiert. Die Finite Elemente Software PLAXIS 2D ermöglicht durch sog. *embedded beam rows* Pfahl- oder Ankerreihen in 2D zu modellieren. In der gegenständlichen Masterarbeit wird die Anwendung dieses Elementtyps im Tunnelbau untersucht. Die Validierung erfolgt dabei mit Hilfe des numerischen Programms *Phase²*. Letztere Software ermöglicht die Modellierung von Ankern basierend auf diversen Modellen. Ein einfaches Tunnelbeispiel ist Gegenstand umfangreicher Parameterstudien. Die resultierenden Ankerkräfte für Ankersysteme in *Phase²* werden dabei mit den Ergebnissen aus PLAXIS 2D (*embedded beam row*) verglichen. Die Ergebnisse zeigen, dass *embedded beam row* eine effiziente Alternative zur Modellierung von *fully bonded, swellex* und *tieback* ist, aber nur bedingt Übereinstimmung mit den Ergebnissen des *plain strand cable bolt* zeigt.

Abstract

Rockbolts are widely used in engineering practice for supporting excavations in rock. Bolt models have been implemented in various numerical methods already, such as FEM (Goodman et al., 1968), BEM (Crotty & Wardle, 1985) and block methods (Cundall, 1971). PLAXIS has implemented the *embedded beam row* feature to primarily model pile rows in 2D. The aim of this thesis is to analyse the possibility of using *embedded beam row* for applications in tunneling. For the validation, the 2D finite element program *Phase*^{2} by Rocscience was selected, due to its capability of modelling different types of rockbolts. A simplified tunnelling problem was modelled in both codes and the results regarding the axial force distribution along the anchors for different types of anchors were compared. The influence of various factors affecting the performance of cable bolts has been evaluated as well. It was concluded that *embedded beam row* can be an efficient tool for modelling *fully bonded*, *swellex* and *tieback* bolts, but it shows limitations in simulating the *cable bolt* behaviour.

Table of contents

List of figures

List of tables

List of symbols and abbreviations

Small letters

$c´$	[kN/m²]	cohesion
c_i	[kN/m²]	cohesion of the interface
p_1	[m]	Radial pressure at $r = r_1$
u_a	[mm]	axial displacement at end point
u_r	[mm]	radial displacement
u_{r1}	[mm]	radial displacement at $r = r_1$
u_x	[mm]	axial displacement
Δu	[mm]	relative displacement
Δu_e	[mm]	elongation of the bolt element

Capital letters

A	[m²]	cross-sectionl area
A_1	[m²]	apparent cable-grout interface contact area
D	[m]	diameter
E	[kN/m²]	Young's modulus
EA	[kN]	axial stiffness
E_b	[kN/m²]	Young's modulus bolt material
F	[kN]	axial force
F_a	[kN]	axial load on cable
$F_{bot,max}$	[kN]	maximum base resistance
F_e	[kN]	axial force
F_{max}	[kN]	base resistance
F_{yield}	[kN/m²]	yield force
G_{soil}	[-]	shear modulus soil
IS	[kN/m²]	interface stiffness for *EBR*

ISF_{RS}	[-]	axial stiffness factor
ISF_{RN}	[-]	lateral stiffness factor
ISF_{KF}	[-]	base stiffness factor
K_b	[kN/m²]	bolt stiffness
k_j^i	[-]	coefficients for cable bolt model
K_F	[kN/m²]	stiffness base
K_{rc}	[kN/m²]	radial stiffnes of the cable
K_0	[-]	initial stress ratio
L_e	[m]	bolt length
L_{pile}	[m]	pile length
$L_{rock\ bolt}$	[m]	rock bolt length
$L_{spacing}$	[m]	out-of-plane spacing
N_{pile}	[kN]	bearing capacity for piles
$N_{rock\ bolt}$	[kN]	bearing capacity for rock bolts
R_{eq}	[m]	equivalent radius
R_{inter}	[-]	interface factor
R_N	[kN/m²]	stiffness axial direction
R_S	[kN/m²]	stiffness lateral direction
$T_{S,max}$	[-]	maximum force axial direction
T_{skin}	[kN/m]	skin resistance
$T_{skin,start,max}$	[kN/m]	skin resistance at the pile top /first point
$T_{skin,end,max}$	[kN/m]	skin resistance at the pile bottom /second point

Greek letters

β	[%]	deconfinement value
γ	[kN/m³]	unit weight
k	[kN]	shear stiffness for the bolt - grout interface
ν	[-]	Poisson‘s ratio
ν_0	[-]	dilation due to splitting

τ_i	[kN/m²]	shear stress of the interface
ϕ	[°]	friction angle
ϕ'	[°]	average coefficient of friction
ϕ_i	[°]	friction angle of the interface
ψ'	[°]	dilatancy angle

1 Introduction

The *embedded beam row* feature in PLAXIS has been developed to model piles in 2D considering a soil-structure interaction. It has been validated as part of a master thesis (Sluis, 2012) in various loading conditions. However, the loads were assumed to be static and the lateral skin resistance was unlimited, so the application of embedded beam row was restricted to a certain pile spacing-diameter ratio. In the PLAXIS version of 2015, a limiting lateral skin resistance has been implemented to deal with laterally loaded piles and piles with larger spacing. Algulin and Pedersen (2014) have applied the *embedded beam row* feature for modelling a piled raft foundation. Van der Kwaak (2015) used *embedded beam row* to simulate the dynamic pile behaviour during earthquake.

The main objective of this thesis is validating the PLAXIS 2D *embedded beam row* for applications in tunneling. The validation is performed by comparison with the finite element program *Phase*^{2}. Five different bolt models have been implemented in *Phase*^{2}: *end anchored, fully bonded, plain strand cable, swellex/split set* and *grouted tiebacks*. For the validation, a simplified tunneling problem was modelled in PLAXIS and *Phase*^{2}. The comparison is done by investigating the axial force distribution along the bolts in both FE-codes.

This short introduction is followed by a chapter focusing on some technological aspects of bolting. The most common bolt types are presented concisely.

The background theory of the bolt models used in *Phase*^{2} is explained in chapter 3. Furthermore, the *embedded beam row* concept is described in detail. Information about the development of the theory used for *Plain Strand Cable* model is given in Appendix A.

Chapter 4 presents the numerical model used in PLAXIS and *Phase*^{2}. 6-noded finite elements are used in both codes, since *Phase*^{2} only provides 6-noded triangular elements. The sensitivity of the results to the mesh coarseness and the element type is afterwards studied in PLAXIS. Two different material models, namely linear-elastic and Mohr-Coulomb are used for modelling the rock. Moreover, the modelling procedure for the different bolt types is described.

In chapter 5, the results from PLAXIS using *embedded beam row* are compared with the results for *fully bonded bolts, swellex, grouted tiebacks* and *cable bolts* from *Phase*^{2}. Parametric studies were performed to evaluate the influence of various factors affecting the mechanical behaviour of cable bolts, as rock properties, stress level and cable geometry. For modelling of *end anchored* bolts, *node-to-node* anchors are used in PLAXIS. The results are shown in Appendix D.

Chapter 5 is followed by a summary of the conclusions and recommendations for modelling of bolts by means of *embedded beam row*.

2 Technological background

Rockbolts and cablebolts are designed to help the rock mass support itself (Rabcewicz, 1964). This is practically achieved by a load transfer mechanism between the ground and the reinforcement through the bonding. All reinforcements consist of four principal components (Windsor, 1996):

- Rock
- Element: the main function of the reinforcing bar is to restrain the deformations of the surrounding ground.
- Internal fixture: the way the reinforcing bar is coupled to the rock.
- External fixture: a plate and a nut.

The mechanical behaviour of the support system is dictated by the interaction of all components. The main difference between rockbolts and cablebolts is the use of a bar or a several-wire strands as a reinforcing element.

2.1 Rockbolting

Based on the anchoring of the rod to the rock or soil, the bolting systems can be classified as follows (Windsor, 1993):

- discretely mechanically or frictionally coupled systems (DMFC);
- continuously frictionally coupled systems (CFC), and
- continuously mechanically coupled systems (CMC).

2.1.1 Discretely mechanically or frictionally coupled systems (DMFC)

DMFC rockbolts are anchored to the rock at the borehole far end, just over a small length, while the rest of the bar is free. They are the earliest and also the simpliest system to come into widest use (Martin, 2012).

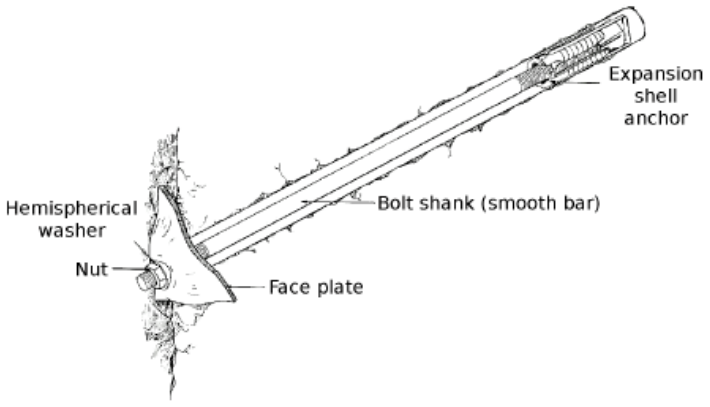

Figure 1: Main components of DMFC rockbolts (adapted from Stillborg 1986)

Anchoring can be achieved using:

- A fast-set resin grout
- Altenatively a slot-and-wedge mechanism
- Or an expansion shell

They are active rockbolts - they can provide immediate support action, what is the principal advantage of them. Besides, the time of installation is quite short. When it comes to the loads, they are not able to deal with shear loads unless the shear displacement exceeds the thickness of the borehole annulus. On the other side, DMFC systems can handle tensile, compressive and bending loads.

Regarding their disadvantages, perhaps the most important is the need to regularly check the proper tensioning of the bar: creep behaviour, vibrations induced by blasting or losening of the face plate can drastically reduce the load on the bar. Furthermore, DMFC systems cannot be used in neither very hard nor very soft rock conditions. Moreover, DMFC systems are more efficient when they are as perpendicular to the strata as possible.

2.1.2 Continuously frictionally coupled systems (CFC)

CFC rockbolts rely on full-length contact to provide the reinforcing frictional action between the bar and the borehole wall. They are very easy to install and can hold a combination of tensile, compressive and bending loads. In addition, they can acommodate large rock deformations, which make them suitable for deep excavation applications (Martin, 2012). Since they mainly provide support action if the surrounding ground tries to deform, they are passive rockbolts.

The most popular friction bolts are Swellex and Split-set, where the bar is metallic.

Split Set rockbolts:

Split-set's main adavantage is the speed and the ease of installation. On the other hand, the risk of corrosion remains one of its main problems, and the borehole requires very specific dimensions and regularity.

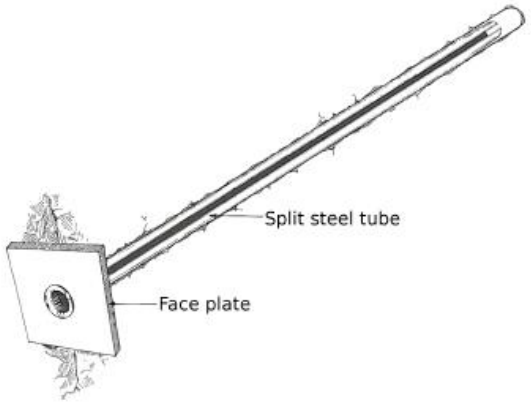

Figure 2: Split-set rockbolt (adopted from Stillborg 1986)

Swellex rockbolts:

The main advantage of the Swellex rockbolt is that it embraces the shape of the borehole, assuring a good contact along its length. The speed of installation is another important asset. In situ, the Swellex bolt is inserted into the borehole with the closed extremity facing the borehole end. High-pressure water (approximately 30 MPa) is then injected inside the folded tube, which thereby inflates and deforms plastically, coming into contact with the borehole walls.

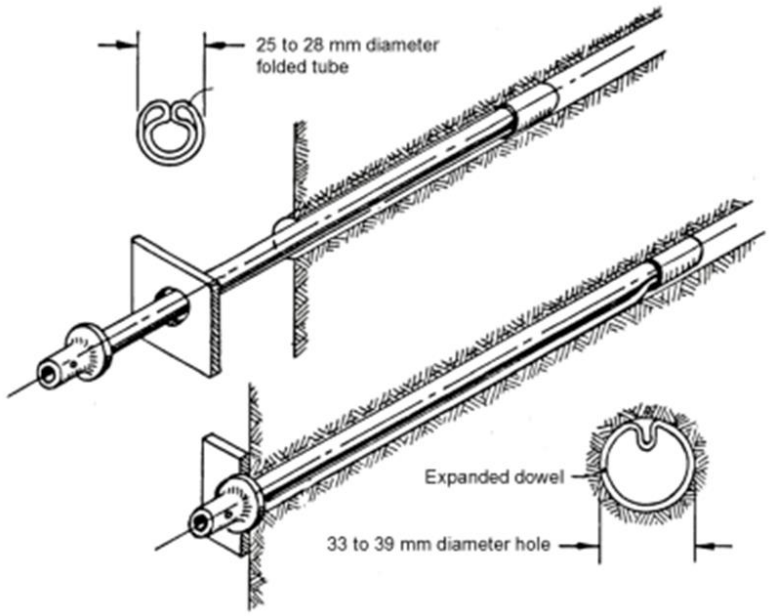

Figure 3: Swellex rockbolt (after Hoek 2007)

2.1.3 Continuously mechanically coupled systems (CMC)

CMC are refered to as fully grouted rockbolts. They are anchored to the rock or soil along their entire length. Since the entire length of the bar is embedded in the grouting material, the risk of corrosion is reduced. CMC rockbolts can be used either as a temporary or a permanent reinforcement. They are able to hold a combination of tensile, compressive, shear and bending loads. Other advantages of those rockbolts are: high flexibility and resistance to corrosion and chemical attacks, high strength-to-weight ratio, electromagnetic neutrality and ease of handling (Martin, 2012).

Fully grouted rockbolts can only provide support action if the surrounding soil or rock mass tries to deform: they are passive anchorage systems.

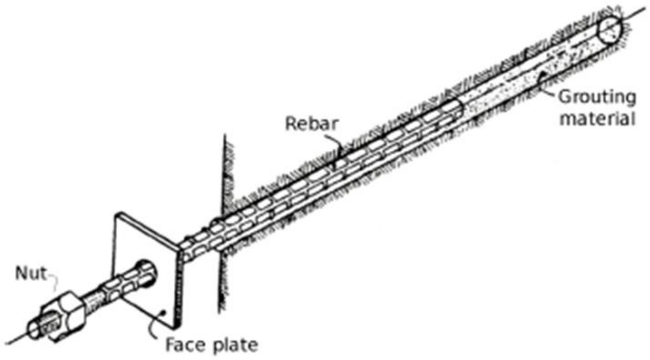

Figure 4: Main components of CMC rockbolts (adopted from Hoek 2007)

2.2 Cablebolting

Cablebolts are based on the same principles as rockbolts. They are normally fully grouted and can sustain tensile, compressive, shear and bending loads. In contrast to rockbolts, cablebolts are made from steel ropes, instead of plain bars. The standard configuration consist of several wires wound around a central wire (plain strand cable bolt). In order to increase the load transfer mechanism , the wires may be rewound to particular structures (e.g. birdcage, nutcage, mini-cage etc). Due to their helical structure, cablebolts are able to hold torsional loads. Furthermore, cablebolts have a higher capacity, compared to the traditional rockbolts.

Another advantage of cablebolts is their flexibility, thus they can be packaged as coils and be easily transported.

Finally, the most important characteristic of cablebolts with respect to rockbolts is the need to use face plates. Cables may rotate under tensile loads, if one of the extremities is left free. As a consequence, the wires tend to untwist themselves and form an dissociated structure (Martin, 2012).

3 Scientific background

3.1 Bolt support models in *Phase²*

Five bolt support models are available in *Phase²*: *End Anchored*, *Fully Bonded*, *Plain Strand Cable*, *Swellex/Split Set* and *Tiebacks*. The bolts are represented by one or a series of 1D elements, which interact with the finite element mesh as individual "bolt elements". Depending on the bolt type, bolt elements may fail in tension (tensile failure), shear (bond failure) or both modes may occur. Failure of a single bolt element does not necessarily cause failure of the entire bolt, except for *end-anchored* bolts. The theory of the bolt support models implemented in *Phase²* is outlined in this chapter. (Rocscience, 2018)

3.1.1 End Anchored Bolt

For the *end-anchored* bolt model, the whole bolt length is considered as a single bolt element (Figure 5). The bolt interacts with the FE-mesh through the endpoints only.

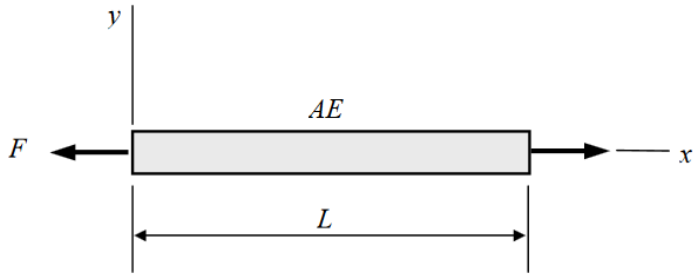

Figure 5: *End Anchored* bolt model (Rocscience, 2018)

The axial force is calculated from the axial displacement as follows:

$$F = K_b \Delta_u \tag{1}$$

where K_b is the bolt stiffness (equal to EA/L) and Δu is the relative displacement between the endpoints.

Failure of *end-anchored* bolts is controlled by the yield strength of the bolt material. Since the end-anchored bolt consists of a single element, failure of the entire bolt occurs if the bolt material has exceeded his tensile capacity. A residual capacity after failure may also be assigned, but in most cases the residual capacity would be equal to zero.

Input parameters for *end-anchored* bolts

The behaviour of *end-anchored* bolts in *Phase*^{2} is defined by the geometry (*Bolt Diameter*) and material properties (*Bolt Modulus E, Tensile Capacity, Residual Tensile Capacity*). Additionally, a *Pre-Tensioning Force* can be specified.

3.1.2 Fully Bonded Bolt

Fully bonded bolts are divided into bolt elements, determined by the intersection of the bolt with the FE-mesh. The bolt elements act independently and influence each other only through their effect on rock mass. Thus, individual bolt elements can fail, independently of neighbouring bolt elements within the same bolt- failure of a bolt element does not lead to the failure of the entire bolt.

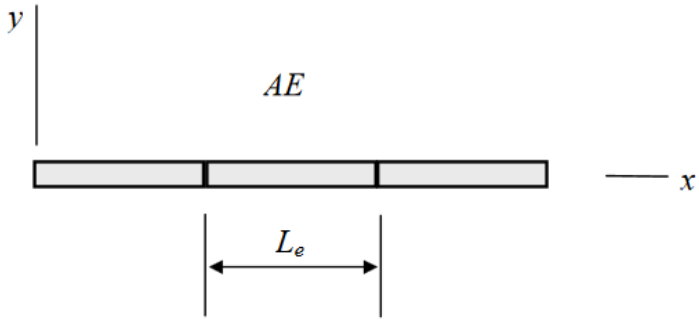

Figure 6: *Fully Bonded* bolt model (Rocscience, 2018)

The axial force is determined from the axial displacement of the bolt element:

$$F_e = \frac{EA}{L_e}\Delta u_e \qquad (2)$$

where L_e is the length of the bolt element and Δu the elongation of the element.

Fully bonded bolts can fail in tension only, if the axial force exceeds the tensile capacity of the bolt material. In *Phase*^{2} it is also possible to define a residual tensile capacity. In this case, the bolt can still carry load (equal to the residual capacity) after exceeding the yield strength (F_{yield}).

Input parameters for *fully bonded* bolts

The information required for modelling of *fully bonded* bolts includes the geometry (*Bolt Diameter*) and the material properties (*Bolt Modulus E, Tensile Capacity, Residual Tensile Capacity*). Same as for *end-anchored* bolts, a *Pre-Tensioning Force* can be specified.

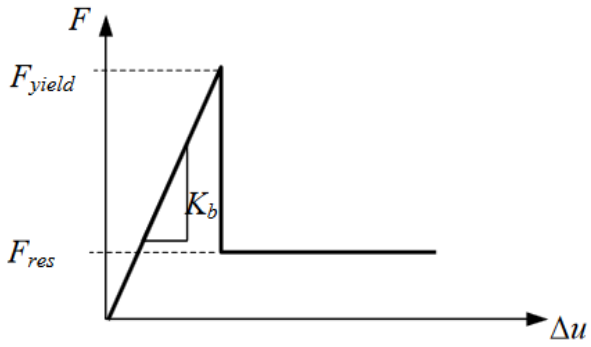

Figure 7: Failure criteria for *fully bonded* bolts (Rocscience, 2018)

3.1.3 Swellex / Split Sets

Swellex / Spilt Sets (also called shear bolts or frictional bolts) consider the shear force due to the relative displacement between the bolts and rock mass, so the shear stiffness of the bolt/rock interface is taken into account. The bolt behaves as a single element. Even though the bolt is divided into elements according to the intersections with the FE-mesh, each element influences the adjacent elements.

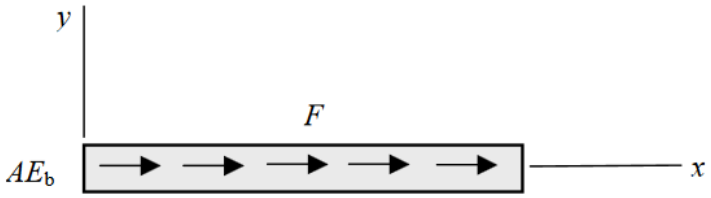

Figure 8: *Swellex / Spilt Sets* model (Rocscience, 2018)

The equilibrium equation may be written as follows (Farmer, 1975, Hyett et al., 1996):

$$AE_b \frac{d^2 u_x}{dx^2} + F_s = 0 \tag{3}$$

where A is bolt cross-sectional area, E_b is the Young´s modulus for the bolt and F_s represents the shear force (per unit length). The shear force is defined as a linear function of the relative displacement between the rock mass and the bolt:

$$F_s = k(u_r - u_x) \tag{4}$$

where k represents the shear stiffness for the bolt-grout interface, usually determined from laboratory pull-out tests.

Swellex/Split Set bolts may fail in two modes: in tension- if the tensile capacity is exceeded, or in shear- if the bond strength is exceeded. By defining a residual tensile capacity, the axial capacity after the axial load in the load has reached the tensile capacity, will be controlled by the residual tensile capacity.

Input parameters for *Swellex / Split Set* bolts

The input parameters required for modelling of frictional bolts include:

- *Tensile Capacity* (only if Plastic Bolt Model is selected for the bolt material behaviour) and *Residual Tensile Capacity*
- *Bolt Modulus*
- *Tributary area* (cross sectional area without the hollow area of the bolt, together with *Bolt Modulus*, it determines the *Axial Stiffness* of the bolt)
- *Bond strength* (the maximum shear force of the bolt / rock interface – can be determined from pull-out tests)
- *Bond shear stiffness* (the shear stiffness of the bolt / rock interface – it represents the slope of the elastic part of the graph on a shear force vs. displacements graph from pull-out tests)
- *Elastic* or *Plastic* material behaviour for the Bolt Model (if *Elastic Bolt Model* is selected, the forces in the bolt are determined by the *Axial* and *Shear Stiffness* of the bolt; if *Plastic* behaviour is selected, the *Bond Strength*, the *Tensile Capacity* and the *Residual Tensile Capacity* are taken into account)

Additionally, the user can simulate *Face Plates* on bolts, add a *Pull Out Force*, add a *Pre-Tensioning Force* and account for the effects of *Rock Joints* on the bolt.

3.1.4 Tiebacks

Tiebacks consist of a free (unbonded) length and a bonded length. The free length behaves as a single element, so the interaction with the FE-mesh is through the endpoints only. If failure of the free length occurs, the entire free length is considered failed. The bonded length is modelled in the same way as Swellex/Split Set bolt, as a series of bolt elements, determined by the intersections with the FE-mesh. Same as for Swellex, the shear resistance for the bonded length is taken into account.

Input parameters for *Tieback* bolts

The necessary input data for Tiebacks includes:

- *Borehole* and *Cable Diameter*
- *Cable Modulus* (Young´s modulus of bolt material)
- *Cable Peak* (tensile strength of the cable)
- *Bond length* and eventually *secondary bond length*

- *Bond strength* (the maximum shear force along the bond length)
- *Bond shear stiffness* (the shear stiffness of the bolt / rock interface)
- *Elastic* or *Plastic* material behaviour for the Bolt Model (same as for *Swellex*)

Furthermore, the user can add a *Pre-Tensioning Force* and also account for the effects of *Rock Joints* on the bolt.

3.1.5 Plain Strand Cable

Due to the intersections of the cable bolt model with the FE- mesh, a number of bolt segment are created. Nevertheless, each bolt segment influences the adjacent elements and the entire bolt behaves as an individual element.

The plain strand cable model considers the stiffness of the grout, as well as the stiffness and strength of bolt/grout interface.The shear stress generated at the cable is defined by the amount of relative slip at the cable/grout interface and the stiffness of this interface.

The only failure mechanism at present is tensile failure of the cable. Failure of the cable/grout may also occurs, but is not considered as a failure mechanism, because as the rock moves, this interface is assumed to be in a plastic state. Failure of grout/rock interface is not considered at present.

Input parameter for *Plain Strand Cable* bolts

The parameters needed for *plain strand cable* bolts are:

- *Borehole* and *Cable Diameter*
- *Cable Modulus* (Young´s modulus of bolt material)
- *Cable Peak* (tensile strength of the cable)
- *Water Cement Ratio*

The shear stiffness in *Phase*^{2} is defined as the slope of the curve in the shear stress vs. shear displacement graph for the bolt and it is in general non-linear. As a result, the shear stiffness changes depending on the shear stress on the bolt. Alternatively, a *constant shear stiffness* can be defined as an input parameter. In this case, the shear stiffness will not depend on the shear stress on the bolt.

Additionally, the user can simulate *Face Plates* on bolts, add a *Pull Out Force*, add *Bulges* and account for the effects of *Rock Joints* on the bolt.

3.2 Embedded beam row in PLAXIS 2D

The pile (rock bolt /grouted anchor) – soil/rock interaction is a fully three dimensional phenomenon, impossible to model realistically in a 2D model. The embedded beam row feature represents a possibility to deal with a row of rock bolts, ground anchors or piles in a 2D plane strain model.

The pile is represented by a Mindlin beam element and is superimposed „on“ the mesh. As a result, the mesh is continuous. The soil interacts with the pile by a special interface, represented by springs in axial and lateral directions along the pile, and a point-to-point interface at the base (Figure 9). The spring forces are limited by the pile capacity, which is an input parameter, consisting of the shaft capacity and base capacity. The principle is illustrated in the figure below.

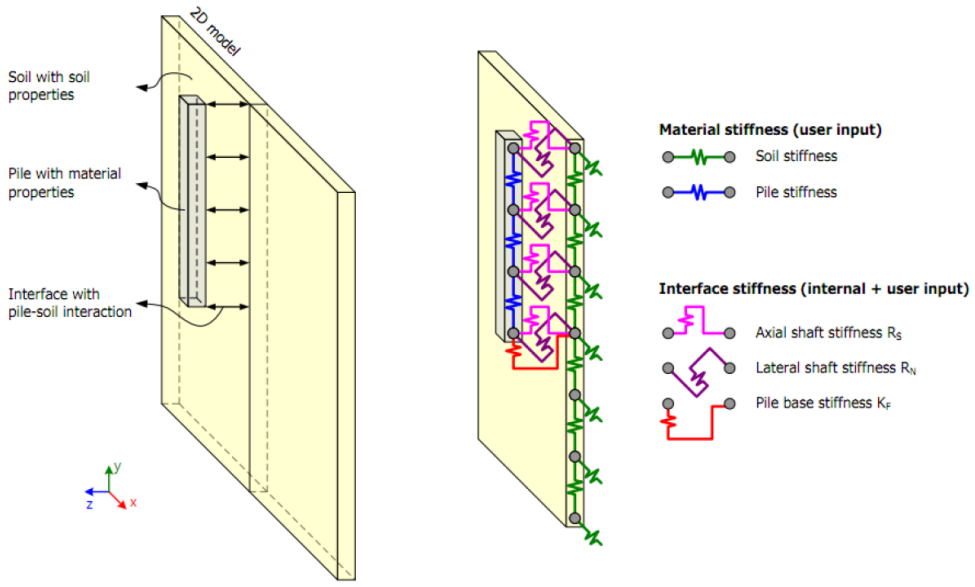

Figure 9: Schematisation of the principle of *EBR* (Brinkgreve et al., 2018a)

When creating embedded beam elements, the special interface elements are created automatically.

PLAXIS offers the possibility to choose between the behaviour of *piles*, *rock bolts* and *grout body*. The three behaviour types differ only with respect to the selection of the connection point.

Regarding the connection of the *EBR* with the solid finite elements, three options are available: *free*, *rigid* and *hinged*. In the first option, the connection point of the *EBR* can move relatively to the soil finite element. If the connection is *rigid*, the relative movement is not allowed. The *hinged* connection allows relative rotation, but no relative displacements. When using *grout body* behaviour, the connection type is automatically set to *free*.

The information required for modelling of rock bolts by means of *EBR* includes the properties of the rock bolt itself, the interaction with the surrounding rock and the out-of-plane spacing.

3.2.1 Beam properties

The material properties for embedded beams are defined by Young´s modulus E and the unit weight of the material γ.

The geometrical properties required for embedded beams include:

- Beam type (predefined/ user defined)
- Predefined beam type (Massive circular beam/Circular tube/Massive square beam)
- Diameter (for Massive circular beam and Circular tube)
- Width (for Massive square beam)
- Thickness (for Circular tube)

3.2.2 Interaction properties

A special interface element is used to model the interaction between the pile/rock bolt and the surrounding soil/rock. The interface behaviour is described by an elastoplastic model. The bearing capacity consists of *Skin resistance* (T_{max}) and *Base resistance* (F_{max}), which are both input parameters. The interface remains elastic, when the shear force does not exceed the skin resistance ($|t_s| < T_{max}$). The elastic behaviour accounts for the displacement differences between the pile/rock bolt and surrounding soil/rock. For plastic behaviour, when the shear force reaches the skin resistance ($|t_s| = T_{max}$), permanent slip may occur.

Since it is a plane strain analysis, the values for skin resistance are automatically divided by the out-of-plane spacing.

Due to lateral displacements, the beam can undergo transverse forces as well. The *Lateral skin resistance*, which is also an input parameter, limits the transverse forces.

The skin resistance

The axial skin resistance and the lateral skin resistance can be defined as *Linear*, *Multi-linear, or Layer dependent* functions.

- *Linear* is mostly applicable in homogeneous soil layers. The pile bearing capacity is then given by:

$$N_{pile} = F_{max} + \frac{1}{2} L_{pile}\left(T_{skin,start,max} + T_{skin,end,max}\right) \quad (5)$$

where F_{max} is the base resistance, L_{pile} the pile length, $T_{skin,start,max}$ the skin resistance at the pile top, and $T_{skin,end,max}$ the skin resistance at the pile bottom.

Rock bolts do not have an end bearing, so the bearing capacity is defined as follows:

$$N_{rock\ bolt} = \frac{1}{2} L_{rock\ bolt}\left(T_{skin,start,max} + T_{skin,end,max}\right) \tag{6}$$

where $L_{rock\ bolt}$ is the length of the rock bolt, $T_{skin,start,max}$ the skin resistance at the first point of the line, and $T_{skin,end,max}$ the skin resistance at the second point of the line.

- The *Multi-linear* option takes into account different properties of multiple soil layers, resulting in different resistances.
- When using the *Layer dependent* option, the local skin resistance is given as a function of the strength properties (*friction angle* φ and *cohesion c*) and the *interface factor*, R_{inter}, of the surrounding soil/rock.

$$tan\varphi_i = R_{inter} tan\varphi_{soil} \tag{7}$$

where τ_i is the local shear stress resistance of the interface, ϕ_i and c_i are the friction angle and the cohesion of the interface, ϕ_{soil} and c_{soil} are the friction angle and the cohesion of the soil/rock, R_{inter} is the strength reduction factor related to the soil layer and $p´$ is the normal stress. In this case the bearing capacity depends on the stress state in the soil/rock.

The skin resistance, T_{skin}, is defined as:

$$T_i = 2\pi R_{eq} \tau_i \tag{8}$$

To avoid undesired high values for the skin resistance, a maximum resistance T_{max} can be defined, which acts as a cut-off value.

This option is available only for the *Axial skin resistance*.

Interface stiffness factor

The *interface stiffness factors* should account for the difference in the displacements between the pile (or rock bolt, or ground anchors) and the soil /rock surrounding the pile.

The interface stiffnesses are defined as follows:

$$R_s = ISF_{RS} \frac{G_{soil}}{L_{spacing}} \tag{9}$$

$$R_N = ISF_{RN} \frac{G_{soil}}{L_{spacing}} \tag{10}$$

$$K_F = ISF_{KF} \frac{G_{soil} R_{eq}}{L_{spacing}} \tag{11}$$

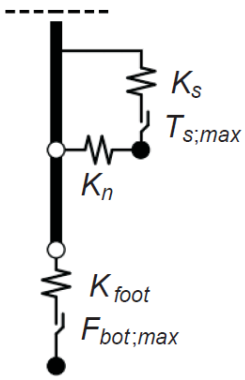

R_N = stiffness lateral direction
R_S = stiffness axial direction
K_F = stiffness base
$T_{s;max}$ = maximum force axial direction
$F_{bot;max}$ = maximum base resistance

Figure 10: Soil structure interaction for *EBR* (Brinkgreve et al., 2018b)

where ISF_{RS} is the axial skin stiffness factor, ISF_{RN} is the lateral skin stiffness factor and ISF_{KF} is the pile base stiffness factor.

The default values of interface stiffness factors are related to the out-of-plane spacing and pile diameter, according to:

$$ISF_{RS} = 2.5 \left(\frac{L_{spacing}}{D}\right)^{-0.75} \tag{12}$$

$$ISF_{RN} = 2.5 \left(\frac{L_{spacing}}{D}\right)^{-0.75} \tag{13}$$

$$ISF_{KF} = 25 \left(\frac{L_{spacing}}{D}\right)^{-0.75} \tag{14}$$

The default values are derived as part of a master thesis study (Sluis, 2012) for bored piles, statically loaded in axial direction. The validation has been performed by fitting with the load-diplacement curves of the Dutch annex of Eurocode for bored piles (for axial loading) and 3D calculations (for lateral loading). Since the derived formulas are not based on physical principles, the default values can be overruled.

4 Numerical Model

For the validation of embedded beam row, a simplified tunneling problem was modelled in PLAXIS 2D and *Phase*^{2}. Tunnel geometry and material properties were taken from Schädlich (Schädlich, 2013). For the calculation, plain strain conditions are assumed. The calculations were performed using 6-noded triangular elements in both codes, since *Phase*^{2} only provides 3 or 6-noded triangular elements. The sensibility of the numerical model to the element type and mesh coarsness was subsequently studied in PLAXIS 2D.

4.1 Model geometry

The same tunnel geometry is used in PLAXIS and *Phase*^{2}. The finite element model has a height and a width of 100m. The circular tunnel, located at the center of the model, has a diameter of 9.4m. The support consists of five anchors of 6m length and a tunnel lining of 20cm thickness. The boundary at the bottom of the model is fixed in all directions, vertical model boundaries are fixed in horizontal direction and the top boundary of the model is free in all directions. The groundwater table is located at the bottom of the model and drained conditions are assumed. Figure 11 shows the model as implemented in PLAXIS and *Phase*^{2}.

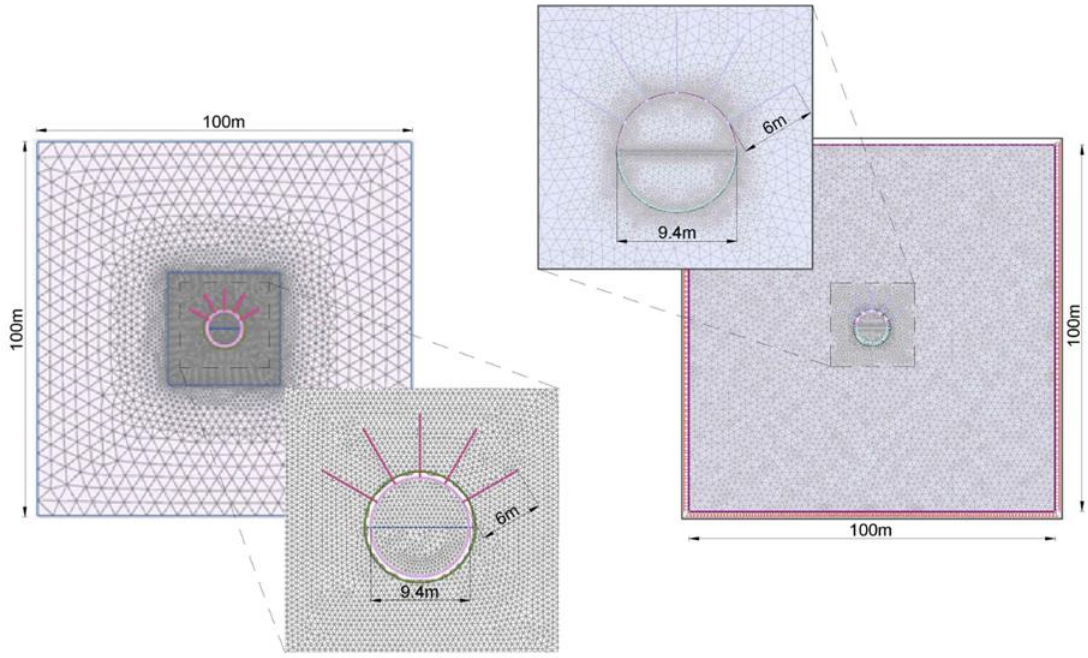

Figure 11: Model geometry in PLAXIS (left) and *Phase*^{2} (right)

4.2 Material parameters

The rock mass properties are summarized in Table 1. The anchor parameters are listed in Table 2. The self-weight of anchors is neglected and the yield strength is considered as the maximum capacity of the anchors. It should be noted that the material parameters for the anchors may differ depending on the anchor type. A detailed outline of the input parameters required for modelling of the different anchors in PLAXIS and *Phase*^{2} is provided in Appendix C.

Table 1: Material parameters for the rock mass

Unit weight	γ	25 kN/m^3
Young´s modulus	E	850 MPa
Poisson´s ratio	ν	0.2
Initial stress ratio	K_0	0.4
Cohesion	$c´$	300 kPa
Friction angle	$\phi´$	28°
Dilatancy angle	ψ	0

Table 2: Material parameters for the anchors

Diameter	$Ø$	0.032
Unit weight	γ	0
Young´s modulus	E	210 GPa
Length	L	6.0 m
Tensile capacity		230 kN
Spacing		1.0 m

The tunnel lining consists of linear elastic plate elements. The Young´s modulus for the shotcrete directly after excavation is assumed as *5 GPa* and for the cured shotcrete *15 GPa.*

4.2.1 Parameters for *Fully Bonded* bolts

Fully bonded anchor elements can fail only in tension if the tensile capacity of the bolt material is exceeded. Since skin failure is not possible, the *skin resistance* of the *EBR* is set to a high value ($T_{skin,start,max} = T_{skin,end,max} = 500$ *MN/m*). The *base resistance* is set to *zero* for all calculations in PLAXIS 2D.

The *interface stiffness factors* in PLAXIS are left to their default values.

The other geometrical and material properties required are as given in Table 2. In 2D plane strain analysis, the *out-of-plane spacing* is also required. The FE-programs will divide internally the stiffness of the anchor by the *out-of-plane spacing* to calculate the stiffness per meter width.

4.2.2 Parameters for *Swellex* bolts

Swellex bolts can fail in tension, as well as in shear if the ultimate skin friction is exceeded. For the *EBR* in PLAXIS, the ultimate skin friction has been defined by a constant distribution of skin friction ($T_{skin,start,max} = T_{skin,end,max} = 5$ *kN/m*). In *Phase*^{2}, the *bond strength* of the *Swellex* bolts is set to *5 kN/m*. This unrealistically low value has been chosen in order to trigger skin friction failure for the given rock properties. Usually, pull-out test are performed to define the input value for this parameter. Since the limiting skin friction is an input parameter, it should be noted that the external bearing capacity cannot be determined from this calculation.

For the shear stiffness, the default values of the *interface stiffness factors* are used in PLAXIS, whereas in *Phase*^{2} the *bond shear stiffness* is set to *100 MN/m/m*, as suggested from *Rocscience*, based on lab and field tests done worldwide.

The other input parameters are calculated according to the parameters given in Table 2.

4.2.3 Parameters for *Tieback* bolts

Tieback bolts consist of a free anchor length and a grout body. The free length of tiebacks in both models is defined as *6m* and the grouted part *4m*. The material properties are as given in Table 2. The free length of tiebacks, which represents the connection between the tunnel lining and the grout body, is modeled by means of *node-to-node* anchor in PLAXIS 2D. As the name implies, the anchor is connected only through the ends to the other elements and in between there is no interaction with the surrounding ground. The grouted part of tiebacks is modelled by means of *embedded beam element*. For the behaviour of *EBR* the option *grout body* is selected. The endpoint of *node-to-node* anchor is then automatically connected to the *EBR*, and not to the surrounding rock (connection type *free*). The interaction with the surrounding rock is provided by the interface elements of the *EBR*.

In practice, the bond length is usually pressure grouted to ensure a rigid contact between the grouted body and the surrounding soil/rock. In PLAXIS the *skin resistance* of the *embedded beam row* is set to a high value (*500 kN/m*) in order to avoid relative movement along the bond length. In *Phase*^{2} the same value is used for the *bond strength*.

For the shear stiffness of the grouted part of the anchor, the default values of the *interface stiffness factors* are used in PLAXIS, and the *bond shear stiffness* is set to *100 MN/m/m* in *Phase*^{2}.

4.2.4 Parameters for *Plain Strand Cable* bolts

The *Plain Strand Cable* model implemented in *Phase²* is based on the model proposed by Hyett (Hyett et al., 1995). In contrast to the other bolt models in *Phase²*, the bolt-grout interface is considered more precisely, taking into account the grout stiffness as well as the strength and stiffness of this interface.

Due to the fact that the *Plain Strand Cable* is based on a rather complex model, it is necessary to examine the differences between PLAXIS and *Phase²*, in order to form a judgement about the possibility of modelling cable bolts by means of *EBR*.

In *Phase²*, the shear stress generated at the cable is defined by the amount of relative slip at the cable/grout interface and the stiffness of this interface. The only failure mechanism at present is tensile failure of the cable. Failure of the cable/grout may also occur, but is not considered as a failure mechanism, because as the rock moves, this interface is assumed to be in a plastic state. Failure of grout/rock interface is not considered at present.

PLAXIS on the other hand, defines the behaviour of *EBR* by the amount of relative displacements at the interface and the interface stiffness. In this case, the relative slip at the interface cannot be taken into account. The relative displacements are refered to the difference in the displacements between the bolt and the surrounding rock. When reaching the ultimate skin resistance (interface elements are modelled as elastoplastic material), permanent slip occurs, indicating failure.

Phase² considers the progressive failure mechanism of the cable bolts. The axial force at the cable is determined according to the stress decrement during the debonding process. The *EBR* cannot take this effect into account, since the interface stiffness is only related to the shear modulus of the surrounding rock.

Furthermore, the grout annulus cannot be modelled when using *EBR*, since the geometry is defined by a single diameter. The influence of the grouting material can therefore not be captured appropriately. From Hyett (Hyett et al., 1995) it is known that the grout effects the load transfer mechanism of cable bolts, not only through the stiffness properties (low w:c ratio increases the cable bolt capacity), but also through the effect of dilatancy/volumetric strains (after cracking of the grout occurs, the individual grout wedges can be radially displaced along the fractures, increasing the pressure at the borehole wall, which in turn generates an additional pressure at the cable/bolt interface, resulting in higher bond strength).

Therefore, it is questionable whether the *embedded beam row* feature is able to show a good performance when modelling *plain strand cable* bolts. Despite the differences in the model formulation, an attempt was made to model cable bolts as implemented in *Phase²* using *EBR*.

Since the formulation of *EBR* in PLAXIS does not allow modelling of the grout annulus, first the influence of the grout on the anchor force distribution was evaluated in *Phase*^{2}. *Phase*^{2} accounts for the grout quality through the *w:c ratio*, which is an input parameter. It is well known that stiffer grouts can increase the cable bolt capacity. This statement was verified by varying the *w:c ratio* of cable bolts in *Phase*^{2} and analyzing the effect on anchor forces. The calculation was performed according to the calculation phases described in the following chapter (chapter 4.3) and using MC plasticity for the rock mass. The geometry of cable bolts in *Phase*^{2} is defined by the borehole diameter and the cable diameter. The standard cable bolt was selected for modelling. The cable diameter is *15.2mm* and the borehole diameter is assumed equal to *38mm*. The other input parameters are as given in Table 2. The results (Figure 12) confirm that the grout quality affects the cable bolt behaviour.

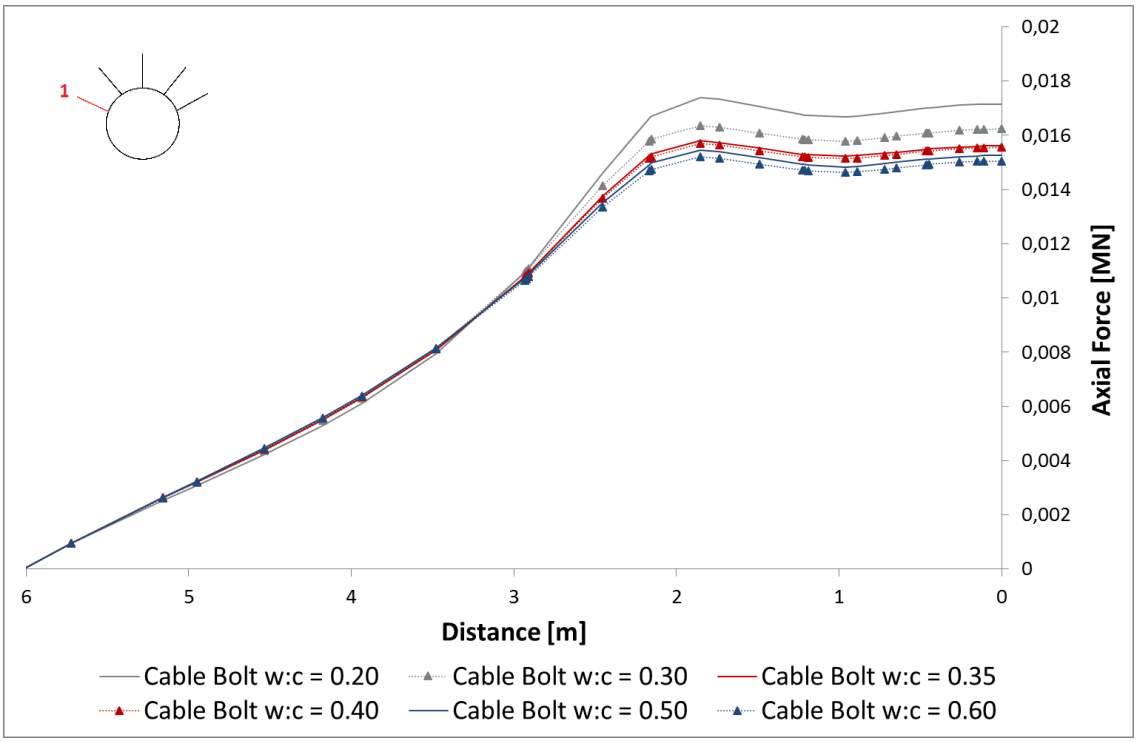

Figure 12: Axial force on anchor 1 in Phase2 for varying w:c ratios

As expected, stiffer grouts yield higher anchor forces. However, for applications in tunneling, w:c ratios between 0.3 and 0.4 are suggested and the influence in this range is minimal, so it can be neglected for this specific problem.

The properties of *EBR* in PLAXIS 2D include the stiffness properties of the cable and the interaction properties with the rock.

Stiffness properties of *EBR* for *Cable Bolts*

For the stiffness of *EBR*, two input parameters should be specified: the *Young´s Modulus, E,* and the cross section geometry. The stiffness of cable bolts is dominated by the axial stiffness of the cable *EA*, since after cracking of the grout body, it will no longer contribute to the axial stiffness of the cable bolt. On the other hand, the geometry is dominated by the grout body, so when specifying the geometry, the diameter of the grout body should be selected. Now, in order to get the actual stiffness of the cable *EA*, a fictious value of *E* was determined, so that the product of the fictious *E* with the cross section area of the grout body, is equal to the stiffness *EA* of the cable. The cable diameter is *15.2mm* and the borehole diameter was assumed as *38mm*, leading to a fictious *E* of *34 GPa*.

Interaction properties of *EBR* for *Cable Bolts*

The interaction properties with the rock involve the *skin friction* and the *interface stiffness factors*.

Skin friction

The skin friction can be defined as *linear*, *multi-linear* or *layer dependent*. For homogeneous soil layers, linear skin friction function can be assumed. Nevertheless, the layer dependent option was also considered for this calculation, since it relates the skin resistance to the strength properties and the stress level in the surrounding rock. To investigate the influence of the *skin resistance* on the behaviour of *EBR*, the calculation was performed with high and low values for the *constant skin resistance*, as well as with *layer dependent skin resistance*. The *interface stiffness factors* are left to their default values. Mohr-Coulomb plasticity is assumed for the material behaviour of the rock. The other material parameters are given in Table 2. The calculation was performed according to the calculation phases as listed in chapter 4.3. As it can be seen from Figure 13 , the results for linear and layer dependent skin resistance are identical when the interface strength is set to rigid.

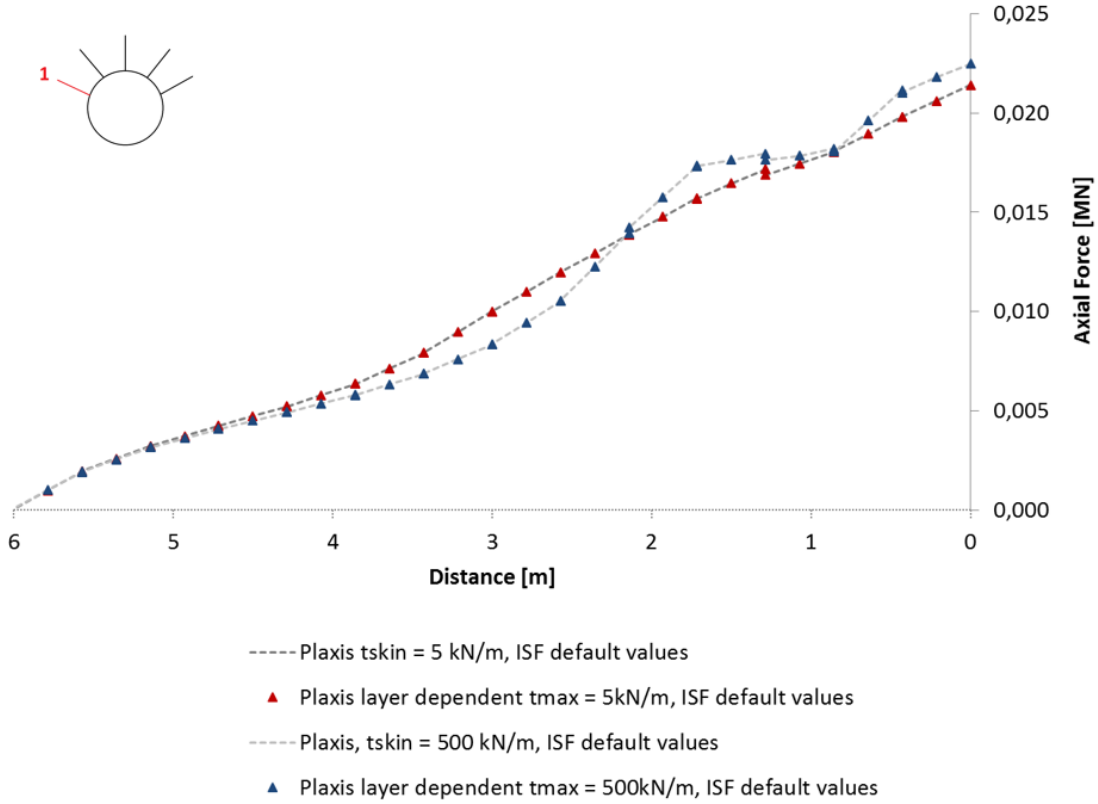

Figure 13: Axial force in anchor 1 for different definitions of skin resistance

The only parameter that influences the behaviour of *EBR* when using layer dependent skin resistance is the strength reduction factor R_{inter}. To study this influence, R_{inter} has been varied from 0 to 1 and the results for the maximum force in anchor 1 are shown in Figure 14.

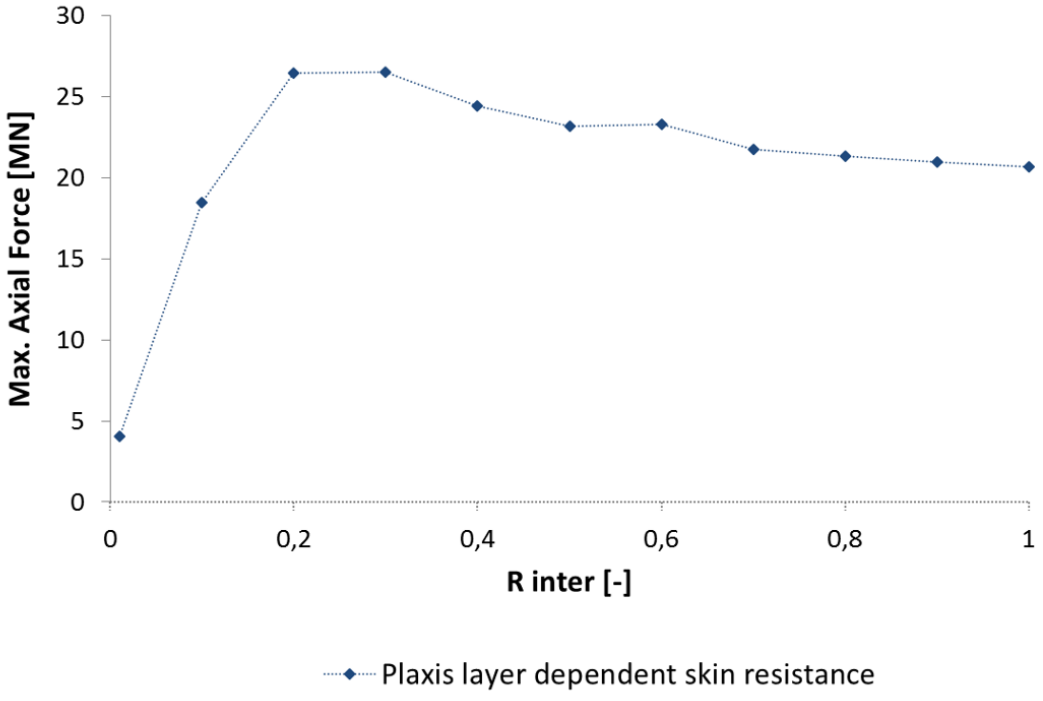

Figure 14: Maximum force in anchor 1 for layer dependent skin resistance

To simulate the interaction anchor/rock, the strength reduction factor R_{inter} can be assumed between 0.7 and 0.8. The influence of R_{inter} in this range is minimal, thus *linear skin resistance* was selected for the further calculations. Since failure of the interface is not considered a failure mechanism in *Phase²*, the *skin resistance* for *EBR* in PLAXIS was set to a high value ($T_{skin,start,max} = T_{skin,end,max} = 500\ kN/m$).

Interface stiffness

The default values for the *interface stiffness factors* (*ISF*) have been derived as part of a master thesis (Sluis, 2012) and are not based on physical principles, but on fitting the load-displacement curve from pile tests with the deformation curve from the Dutch annex of EC7. Therefore, the *ISF* can be overruled to manipulate the relative displacements between EBR and surrounding ground. The determination of reasonable values for the *interface stiffness factors* (*ISF*) is essential in order to obtain a realistic representation of the behaviour of cable bolts, since they control the relative displacements between the *EBR* and the rock and consequently the shear stress generated at the cable. In *Phase²*, the amount of shear stress generated at the cable is controlled by the *shear stiffness* of the cable/grout interface. Therefore, for modelling of cable bolts in PLAXIS, the assumption was made that the *interface stiffness* of the embedded beam elements should be equal to the *shear stiffness* in *Phase²*. The *shear stiffness* in *Phase²* is defined as the slope of the curve in the shear stress vs. shear displacement graph for the bolt and in general it is non-linear. As a result, the *shear stiffness* will change depending on the shear stress. In this case (*variable shear stiffness*), the interface shear stiffness is internally calculated and is a function of the grout quality, the surrounding rock properties and the stress level. It also considers if the grout is cracking as well as if the fractures are open, closed, or partially open. Alternatively, a *constant shear stiffness* can be defined as an input parameter. Consequently, the shear stiffness will not depend on the shear stress. Of course, the calculation with *variable shear stiffness* reflects the real behaviour of cable bolts more accurately, but in this case no correlation to the interface stiffness in PLAXIS is possible. Therefore, the basic idea for the modelling was to perform the calculation in *Phase²* using *variable shear stiffness*, in order to get the relatively realistic axial force distribution and then determine the *constant shear stiffness* to fit the former. The value of the *constant shear stiffness* is afterwards used in PLAXIS to define the *interface stiffness factors* for the *EBR* according to equations (9) and (10). The calculated *ISF* are the input parameters for *EBR*. The assumption is subsequently verified with parametric studies, to evaluate the influence of the factors that affect the interface shear stiffness.

4.3 **Calculation phases**

In order to simulate the tunnel construction process according to the New Austrian Tunnel Method (NATM), the construction process is divided into two stages. In the first stage, the top heading is excavated, followed by the installation of the tunnel lining and anchors. In the second stage, the invert is excavated and subsequently the tunnel lining is installed. To simulate the construction process in PLAXIS, the ß- method is used. Figure 15 and Figure 16 illustrate the calculation phases performed in PLAXIS and *Phase*^{2}, respectively. Five calculation phases are performed in both codes:

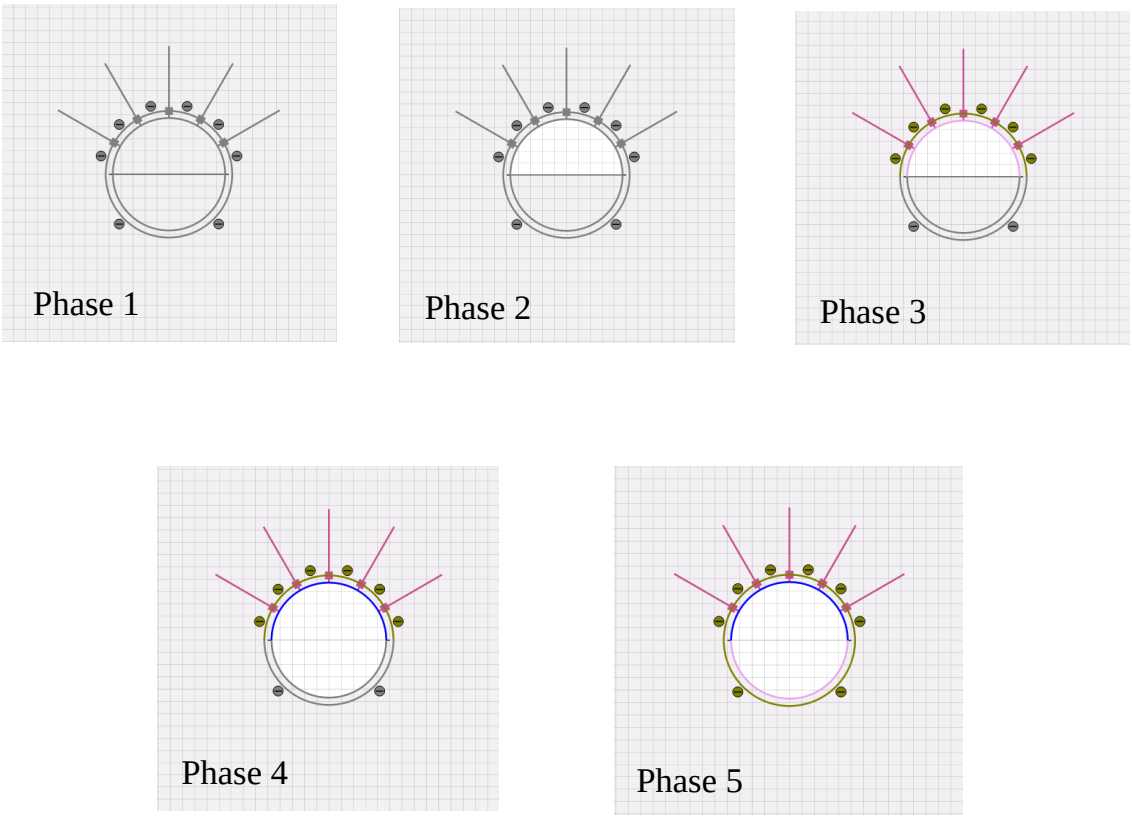

Figure 15: Calculation phases in PLAXIS

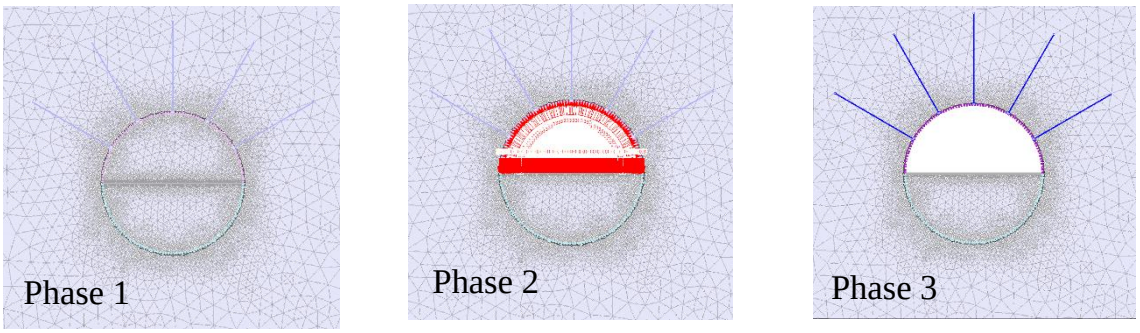

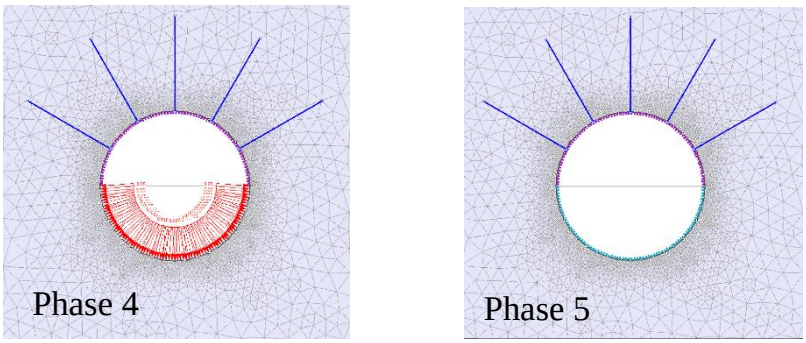

Figure 16: Calculation phases in *Phase*[2]

1.**Initial phase**

The initial stress field is generated using the K_0 *procedure*, with the K_0 - value of 0.4.

2.**Pre-relaxation of top heading**

The value of deconfinement (β-value) for the top heading is assumed as 0.3. The initial stress acting around the tunnel is divided in two parts. 70% of the load acts on the unsupported tunnel, while the other part (30%) should be carried by the support in the next calculation phase.

3.**Excavation of top heading**

The top heading is de-activated and the support consisting of the tunnel lining („young“) and anchors is activated.

4.**Pre-relaxation of invert** (top heading lining „old“)

For the invert, ß-value is assumed as 0.65. 35% of the stresses acts on the unsupported invert, while 65% should be carried by the support in the last calculation phase. Moreover, the material properties of the tunnel lining are modified – top heading lining is set to „old“.

5.**Excavation of the invert**

In the last calculation phase, the invert is de-activated and additionally the invert lining („young“) is activated.

4.4 Influence of the lining discretization

PLAXIS and *Phase*^{2} show some differences concerning the tunnel lining discretization. The tunnel lining in PLAXIS 2D is discretized into curved beam elements, whereas *Phase*^{2} uses straight beams. To evaluate the influence of this differences, the calculation is performed without anchors first. The rock mass is modelled as linear-elastic material, as well as using Mohr-Coulomb failure criterion. The results for the axial forces in the tunnel lining are shown in the Figure 17 and Figure 18.

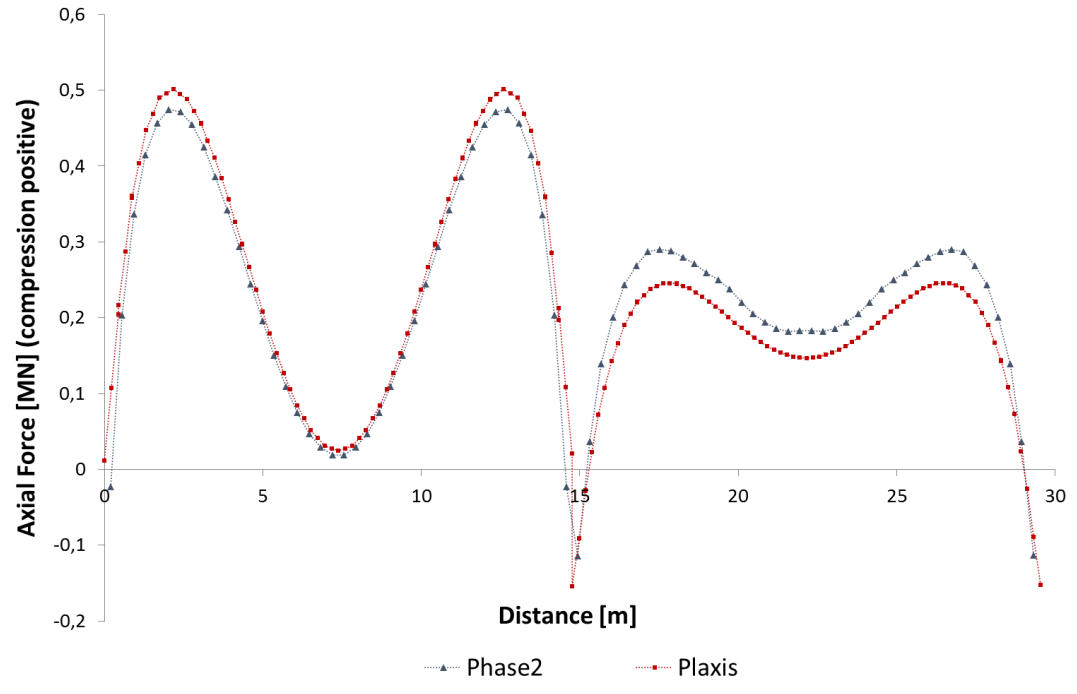

Figure 17: Normal force in the tunnel lining (linear-elastic rock, no anchors)

The normal force distribution in the tunnel lining for linear-elastic rock (Figure 17) shows a good agreement between the two codes for invert forces, while some differences are notable for top heading forces. Thus, the calculation in *Phase*^{2} yields higher top heading forces. In order to get a better approximation, a larger number of elements should be used for the discretization of the tunnel lining in *Phase*^{2}.

Figure 18 illustrates the tunnel lining force distribution for MC rock mass. Compared to the calculation with linear-elastic rock, the normal forces in the top heading increase and invert forces decrease in both codes. As it can be seen from Figure 18, reasonable agreement between PLAXIS and *Phase*^{2} is achieved for MC rock. The top heading forces fit well and only a slight difference can be seen in the

invert lining force distribution. Therefore, the influence of different lining discretizations has been neglected for the further calculations.

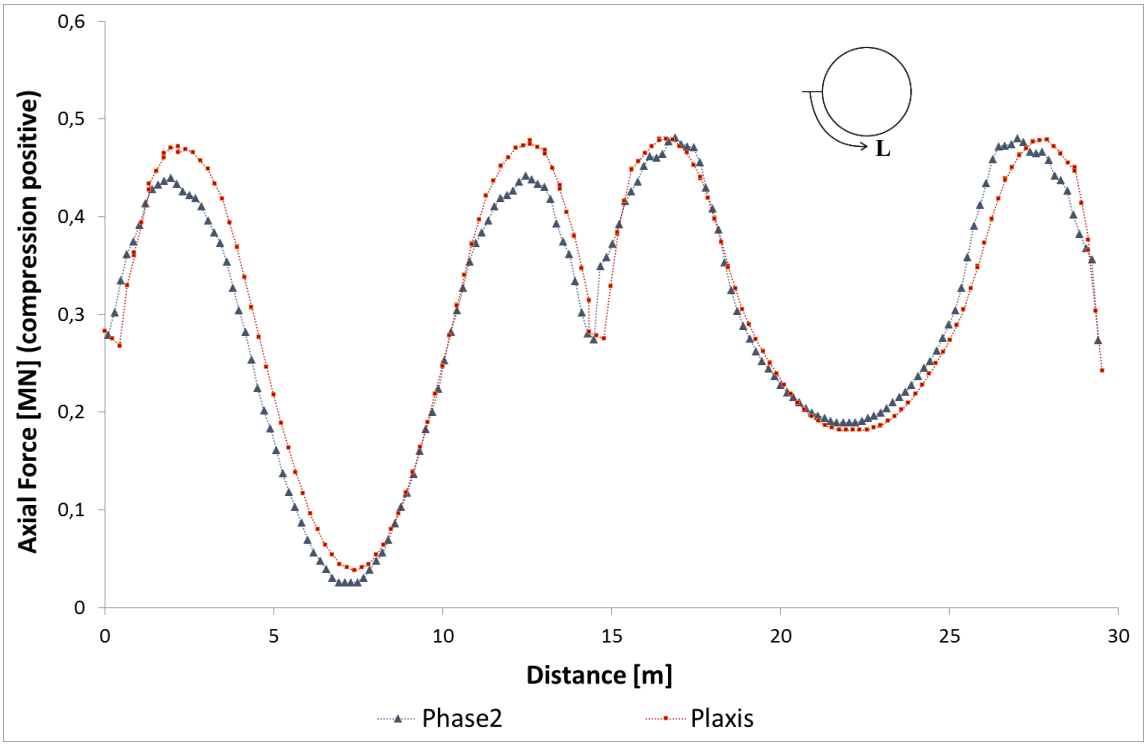

Figure 18: Normal force in the tunnel lining (linear-elastic rock, no anchors)

4.5 Influence of element type and mesh coarseness

As previously mentioned, for the comparison of the results between PLAXIS and *Phase*^{2}, 6-noded triangular elements are used in both codes, since *Phase*^{2} provides only 3 or 6-noded triangular elements. To study the influence of the element type on the results, additionally a calculation using 15-noded elements was performed in PLAXIS 2D. Furthermore, the mesh was varied from a very coarse to a very fine mesh and the effect on the tunnel lining and anchor forces was investigated. The anchors were modelled as described in chapter 5.1, assuming an unlimited bond strength.

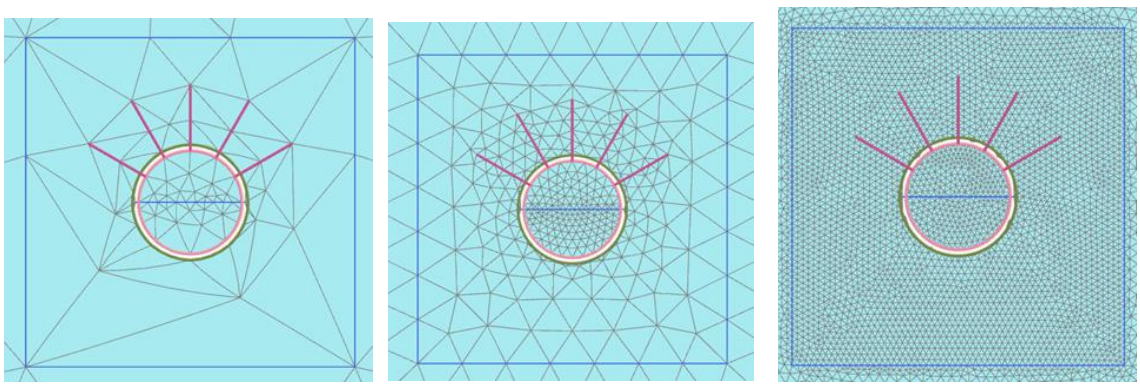

Figure 19: Different mesh discretizations in PLAXIS (very coarse, medium, very fine)

Figure 19 illustrates the different finite element meshes generated in PLAXIS 2D. Figure 20 shows that the mesh coarseness and the element type do not affect the tunnel lining force distribution significantly.

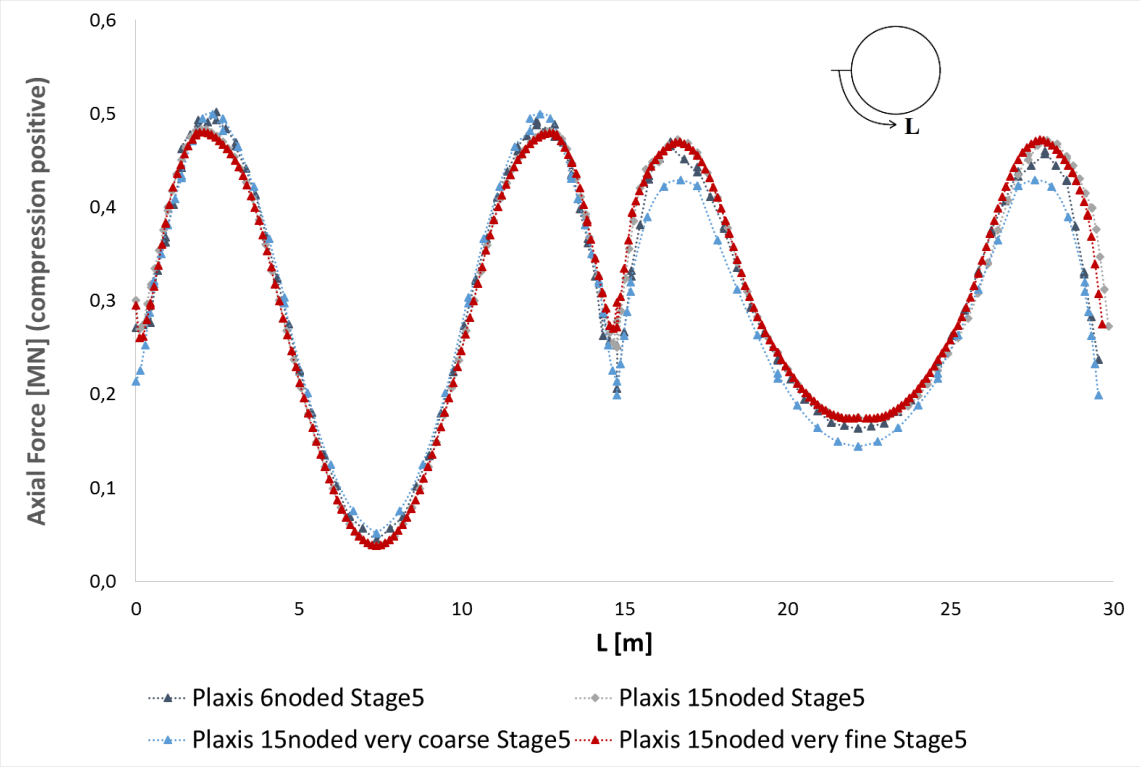

Figure 20: Normal force in the tunnel lining (rock MC, no anchors)

Nevertheless, the mesh coarseness influences the anchor force, particulary if the anchor is affected by plastic points (Figure 21), as for anchor 1. The maximum forces on anchor 1 are in the same range, but the force distribution differs, if very fine mesh is used. So, a plateau of constant force can be observed close to the lining, while very coarse mesh and 6-noded elements yield a linear normal force distribution along the anchor (Figure 23). This behaviour can not be seen for anchor 4, which is located outside the plastic zone.

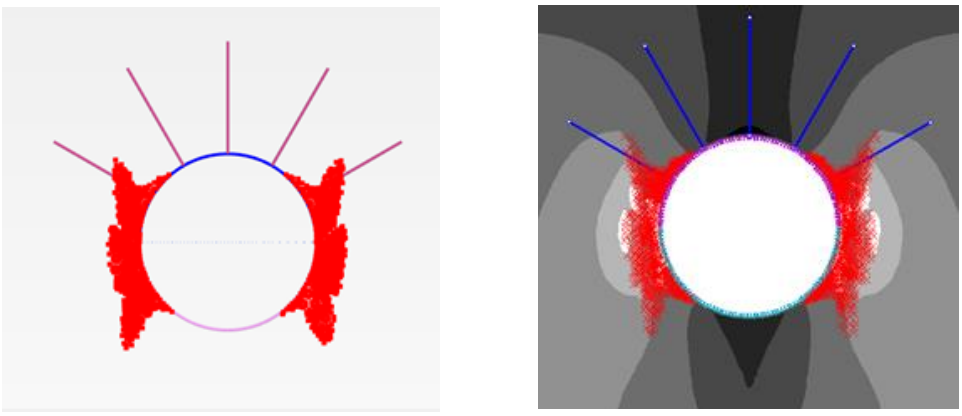

Figure 21: Plastic point history in PLAXIS (left) and *Phase*^{2} (right)

A closer look at the plastic points around the tunnel after top heading excavation reveals the development of some „cherry pit“ mechanism in the very fine mesh. The very coarse mesh on the other hand, produces a rather diffuse plastic zone (Figure 22).

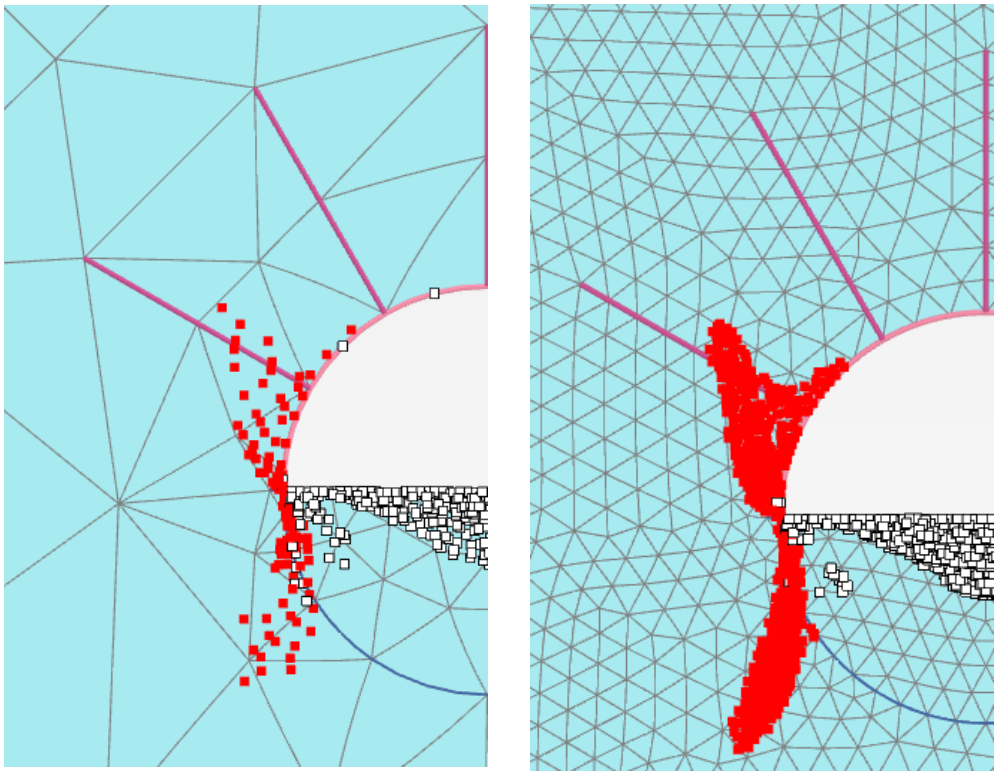

Figure 22: Plastic points after excavation of top heading, coarse and very fine mesh

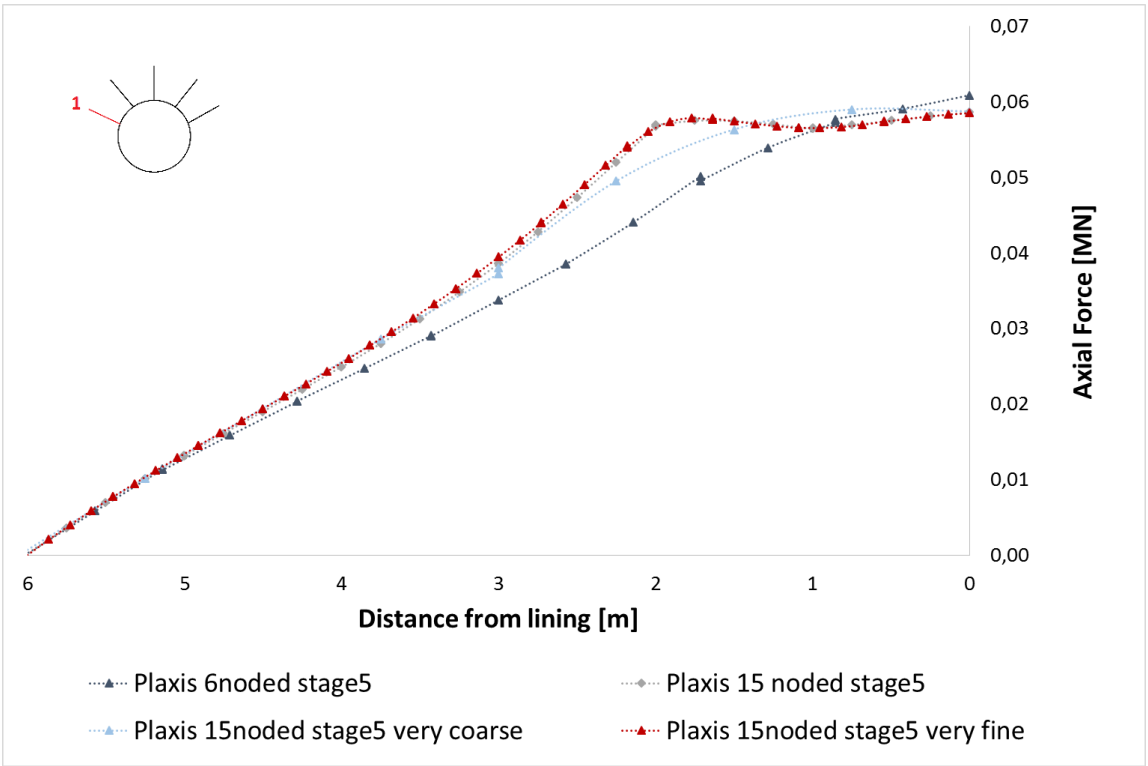

Figure 23: Axial force on anchor 1 for 6-noded vs. 15-noded elements (rock MC)

The influence of mesh coarseness and element type can be seen on anchor 4 as well (Figure 24). Although the normal forces follow the same path, the very coarse mesh and 6-noded elements show higher normal forces in anchor 4.

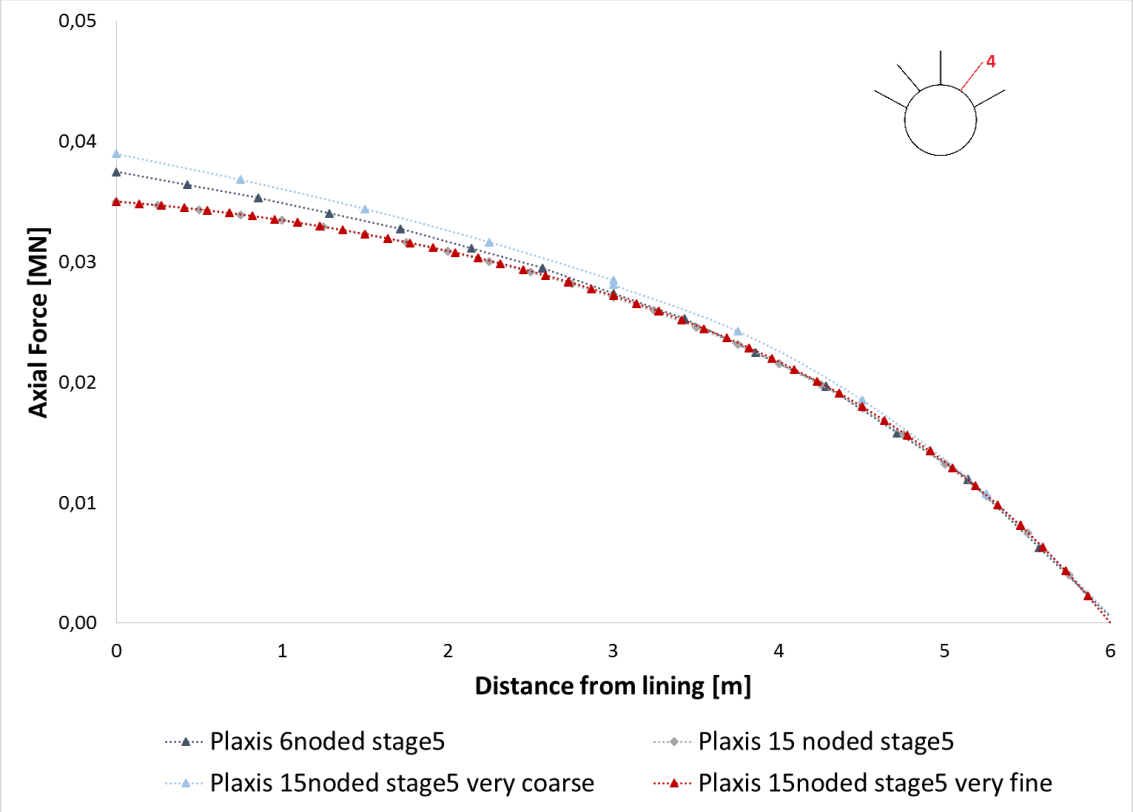

Figure 24: Axial force on anchor 4 for 6-noded vs. 15-noded elements (rock MC)

Due to the influence of the mesh coarseness on the results, very fine mesh was generated for all the further calculations.

5 Validation of the PLAXIS *EBR* by comparison with *Phase²*

In this chapter, the results from PLAXIS for different anchor types are compared with the results from *Phase²*. For the validation of *fully bonded* bolts, the rock mass was modelled as *linear-elastic material* as well as using *Mohr-Coulomb failure criterion*. For the other rock bolt types Mohr-Coulomb plasticty was assumed for the rock mass. The parameters for the different bolt models are described in the previous chapter. The comparison is done by investigating the axial force distribution along the anchors.

5.1 Fully Bonded bolts

As mentioned in the previous chapter, the *skin resistance* of the *embedded beam row* elements is set to a high value in order to simulate *fully bonded* bolts. In Figure 25 and Figure 26 the normal forces in two anchors with respect to radial distance are plotted, for various excavation stages. Linear-elastic material behaviour is assumed for the rock mass.

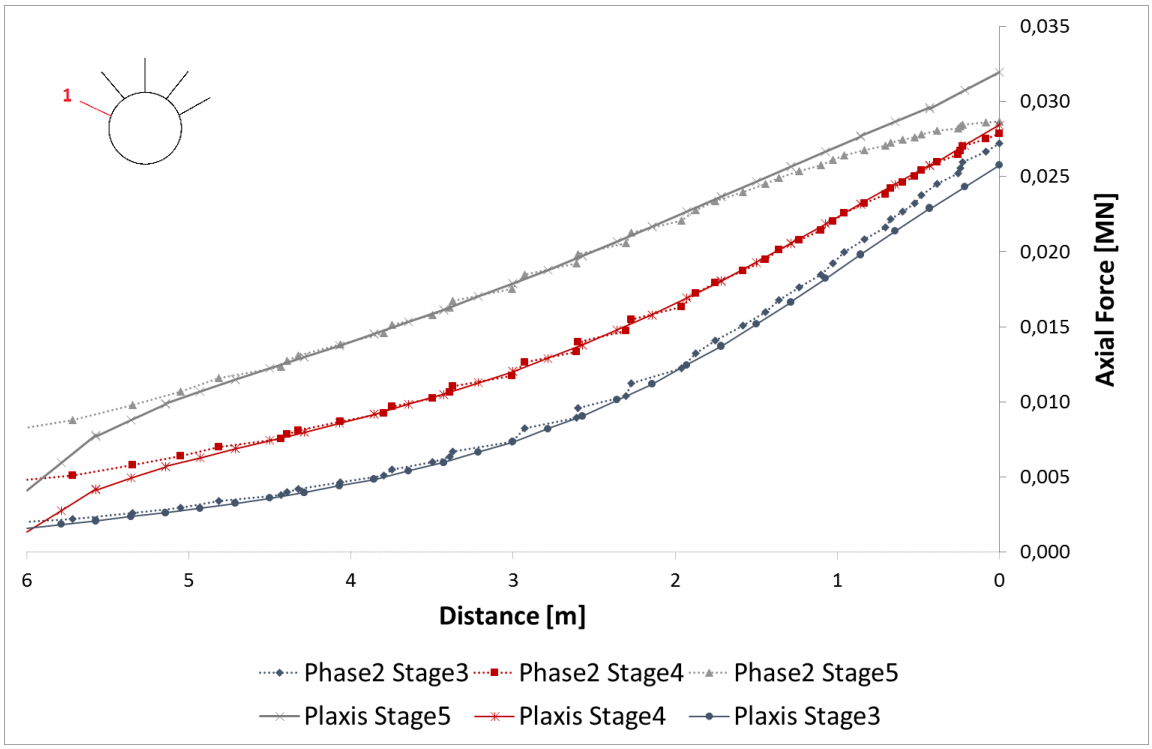

Figure 25: Comparison of axial force distribution for anchor 1 (linear-elastic rock)

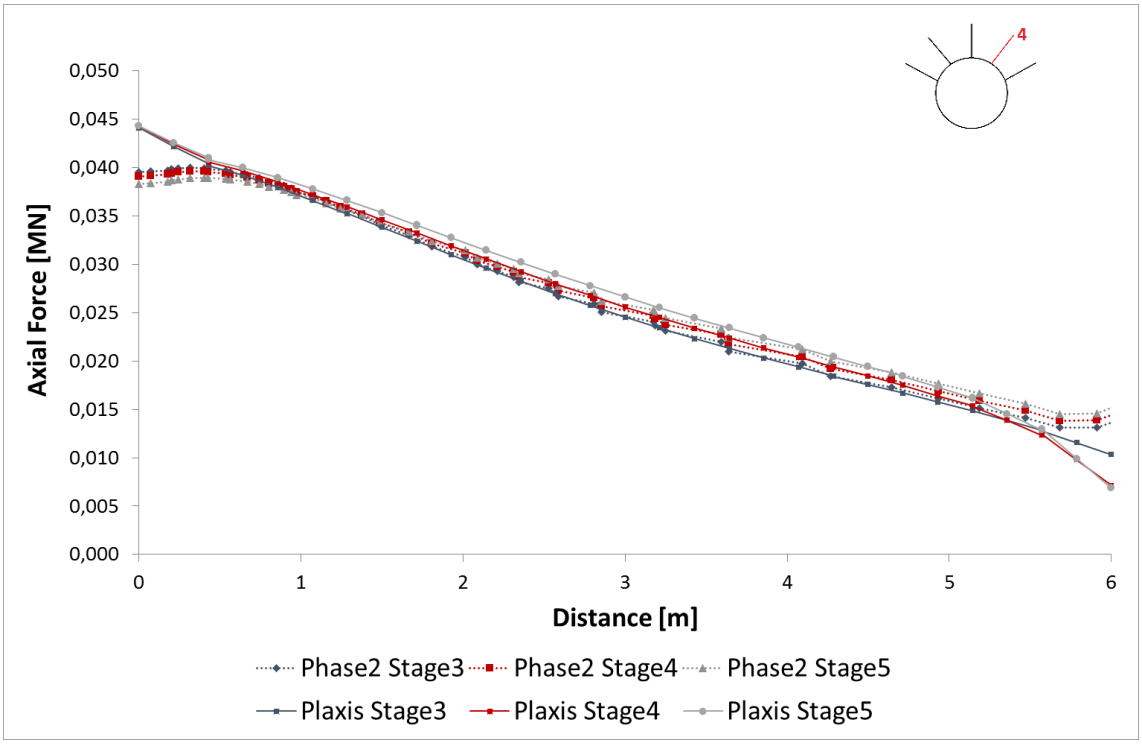

Figure 26: Comparison of axial force distribution for anchor 4 (linear-elastic rock)

As it can be seen, the results from PLAXIS are similiar to those computed in *Phase*^{2}. The maximum anchor force occurs at the tunnel lining and decreases with increasing distance to the lining. Discrepancies are observed at the end of the anchors where anchor forces in PLAXIS tend to zero, whereas in *Phase*^{2} a residual anchor force is present, probably due to a lack of tension cut-off in *Phase*^{2} (Schädlich, 2013).

In Figure 27 and Figure 28 the axial forces for anchor 1 and anchor 4 from calculations in PLAXIS are compared with the results obtained from *Phase*^{2} for MC rock mass.

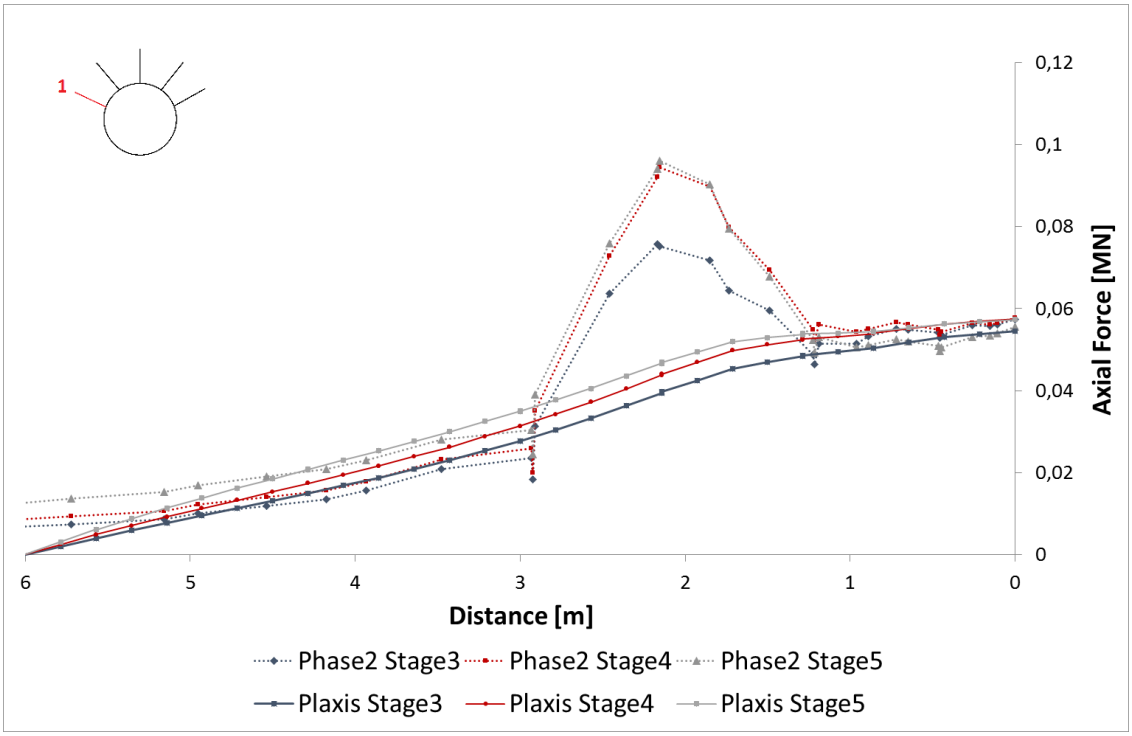

IFigure 27: Comparison of axial force distribution for anchor 1 (MC rock)

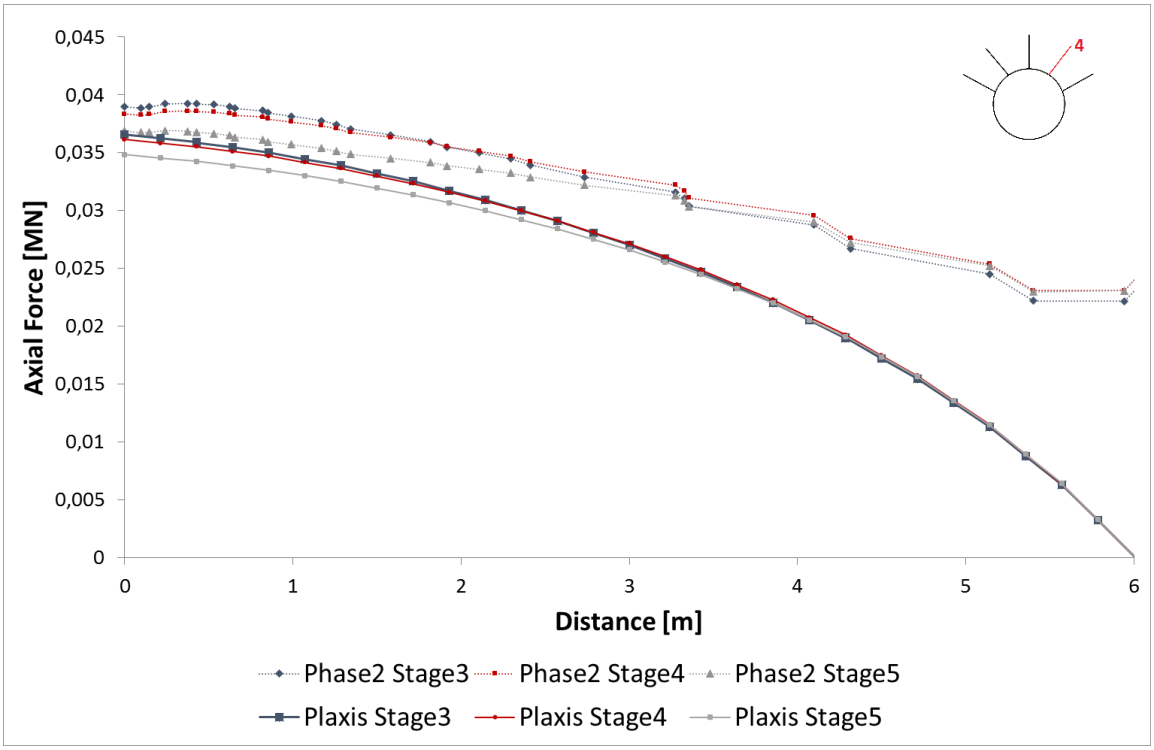

Figure 28: Comparison of axial force distribution for anchor 4 (MC rock)

The normal forces in both codes follow a similiar path, but a notable spike is observed in *Phase²* for anchor force 1 at ~1.5m distance to the lining. Such behaviour can neither be seen in PLAXIS results, nor in the axial force of anchor 4, which is situated outside the plastic zone (Figure 29), nor in the results for linear-elastic rock mass (Figure 25).

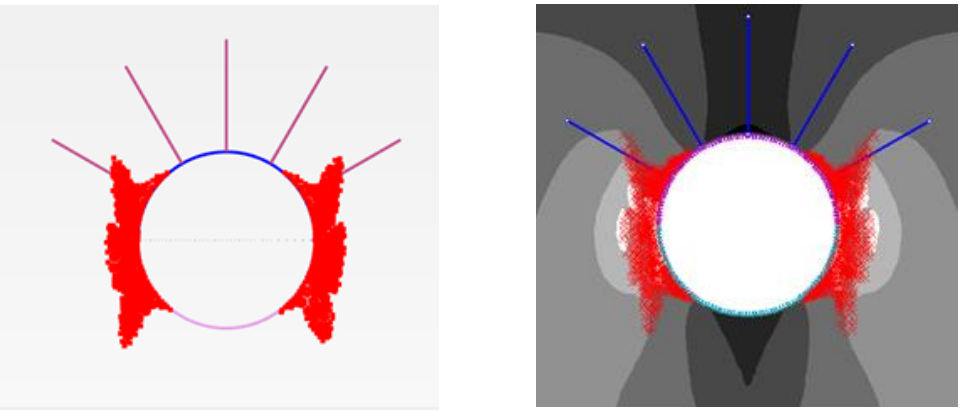

Figure 29: Plastic point history in PLAXIS (left) and *Phase²* (right)

This indicates that the reason for the spike is plasticity in the rock mass. It seems like *Phase²* facilitate the development of complex failure mechanisms, which control the mobilization of anchor forces (Schädlich, 2013).

For the comparison of plastic points (Figure 29), the plastic point history was chosen for the display of the PLAXIS results, since *Phase²* shows in each calculation phase all stress points that reached failure at any previous or the current calculation phase. Only a slight difference between both codes can be seen regarding the plastic points around the tunnel excavation.

5.2 Swellex

The skin resistance of *EBR* in PLAXIS was reduced to *5 kN/m* in order to simulate interface slip at the anchors for the given rock mass properties. The rock mass was modelled with MC. Figure 30 and Figure 31 compare the axial force distribution calculated by PLAXIS with the solution for *Swellex*, calculated by *Phase*^{2}. The results are shown only for the last stage (end of the tunnel excavation) since the other stages are almost identical.

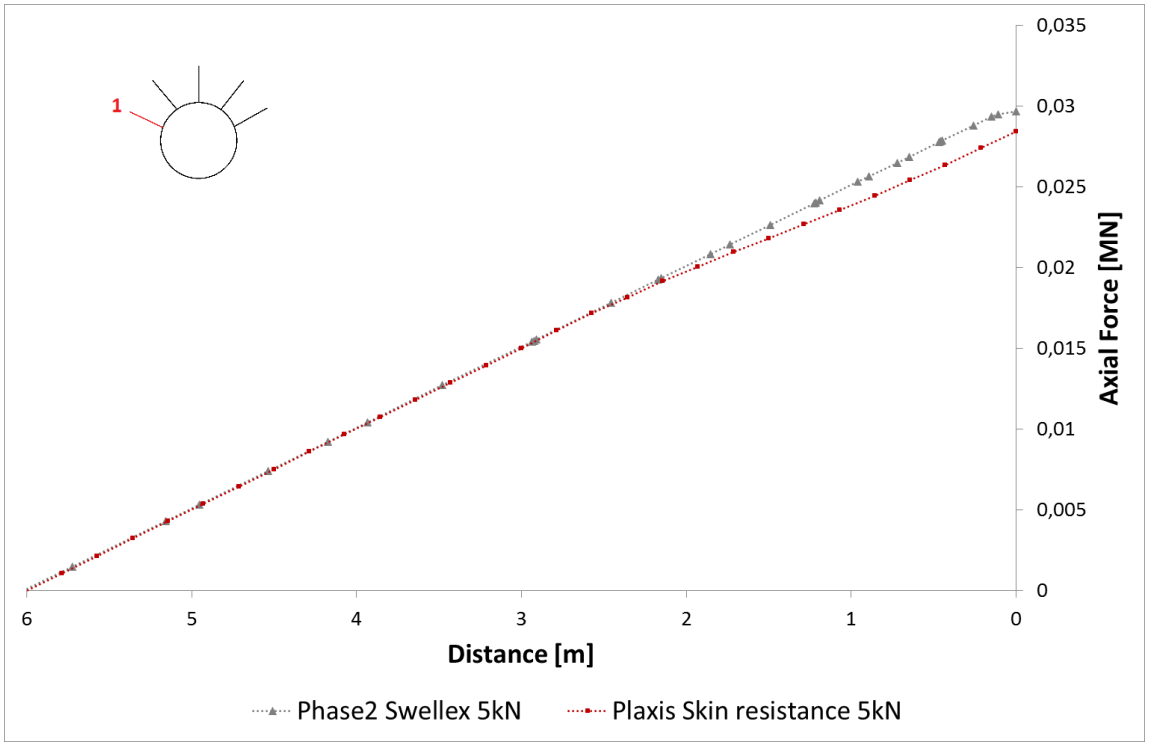

Figure 30: Normal force on anchor 1- Swellex bolts (rock MC)

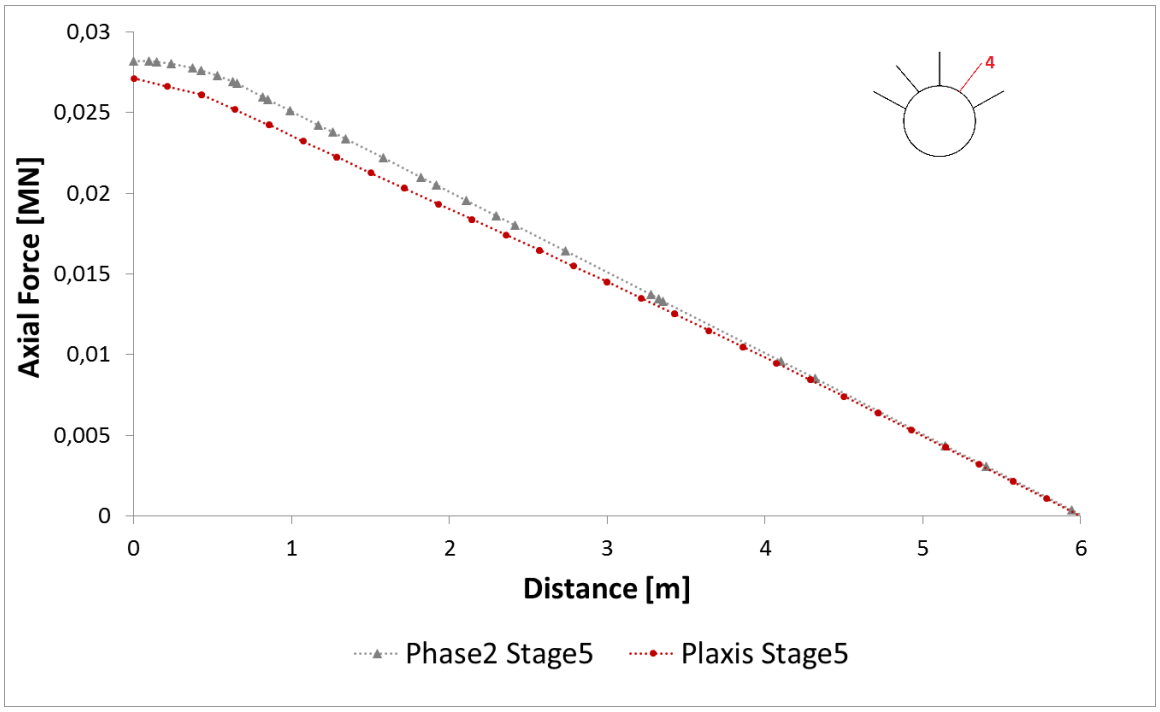

Figure 31: Normal force on anchor 4- Swellex bolts (rock MC)

As it can be seen that the results from PLAXIS are in very good agreement with *Phase*^{2}. The skin friction is fully mobilized along the anchor length, resulting in a maximum normal force of ~30 kN. Due to the constant skin friction, the axial force distribution is approximately linear.

5.3 Tiebacks

In order to simulate the behaviour of grouted anchors, the tieback bolt type was selected in *Phase*^{2}, whereas in PLAXIS the free length was modelled using *node-to-node* anchor and the grouted length using *EBR*. The rock mass was modelled with MC material model. The results obtained from PLAXIS and *Phase*^{2} are illustrated in Figure 32.

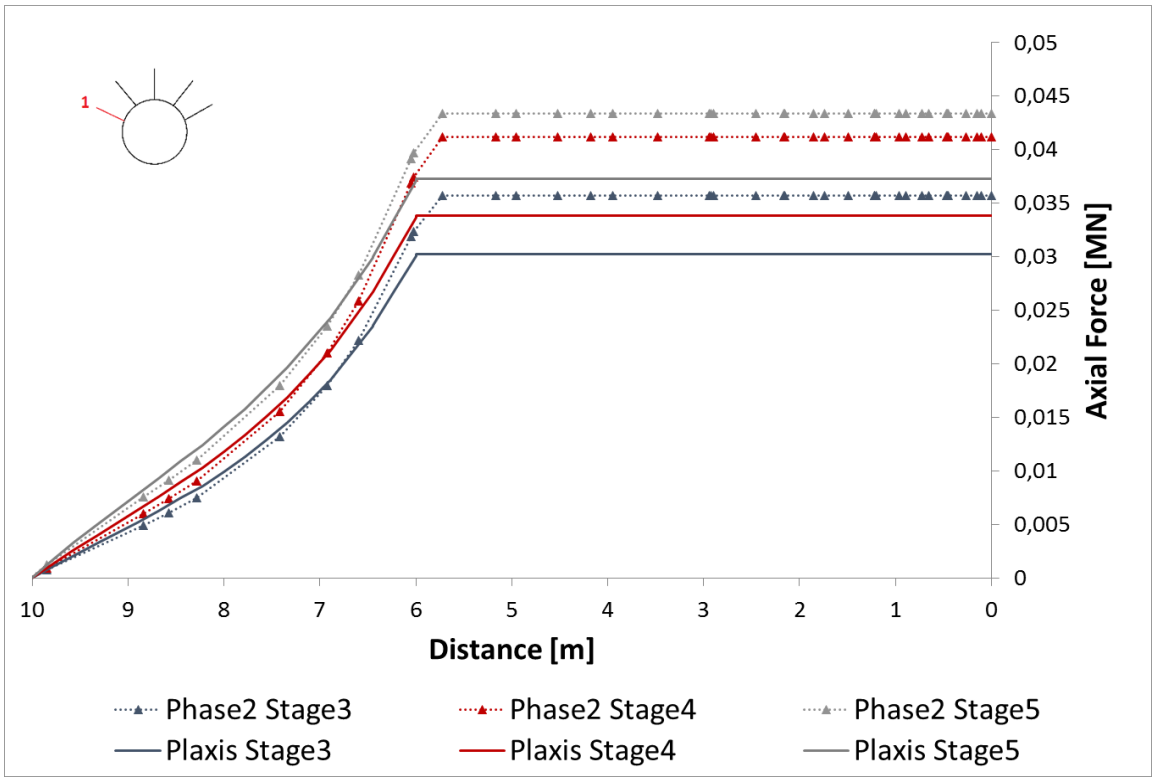

Figure 32: Axial force on anchor 1 – Tiebacks (rock MC)

It can be seen that the axial force distribution along the fixed length is similiar in both codes. The calculation shows some differences in the axial force along the free length, where a lower anchor force is revealed in PLAXIS. The deviation of the forces could be related to the slightly different bond lengths. Thus, the *bond length* in *Phase*^{2} is slightly larger than the emdedded beam element length in PLAXIS and a higher axial force is generated along the bond length in *Phase*^{2}, which is eventually transferred along the free length.

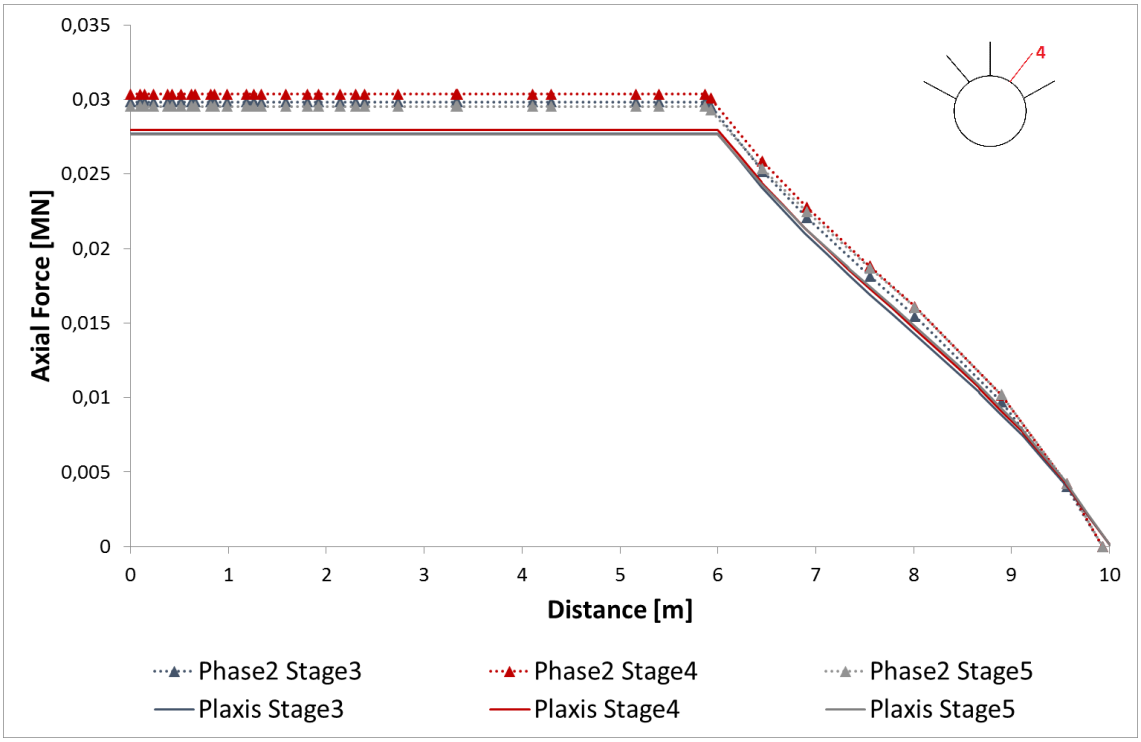

Figure 33: Axial force on anchor 4 – Tiebacks (rock MC)

5.4 Plain Strand Cable bolts

As mentioned in chapter 4.2.4, the determination of suitable values for the *interface stiffness factors* in PLAXIS 2D is essential, due to the fact that they control the relative displacements between *emdedded beam row* and the surrounding rock, and consequently the shear stress generated at the cable. To study the influence of the varying shear stiffness on the behaviour of the bolt, several calculations were performed in both codes. The rock is modelled using MC material model. The necessary input parameters for the anchors are provided in Appendix C.

The shear stiffness is varied from *5* to *100 MN/m/m*. For each constant shear stiffness value, the corresponding value of *ISF* in PLAXIS 2D is calculated, which serves as input parameter for *EBR*. Furthermore, a calculation is performed in *Phase*^{2} considering the *variable shear stiffness*. Since in this case the shear stiffness depends on the shear stress generated at the cable, it is assumed that the relatively most accurate solution is obtained with variable shear stiffness.

The results from both codes for anchor 1 are shown in Figure 35. In general, the results from *Phase*^{2} show a plateau in the normal force distribution close to the lining, whereas in PLAXIS the normal force is distributed almost linearly along the anchor length (Figure 35). When defining high values for the shear stiffness, the behaviour of the *EBR* in PLAXIS still follows the same path as for low shear stiffness – maximum force occurs at the lining and decreases toward the end of the anchor. On the other hand, in *Phase*^{2} a peak at about *2m* distance from the lining is notable, which increases with increasing shear stiffness. This phenomen is revealed only at anchor 1 which is located in the plastic zone and can not be seen neither in anchor 1, nor in PLAXIS.

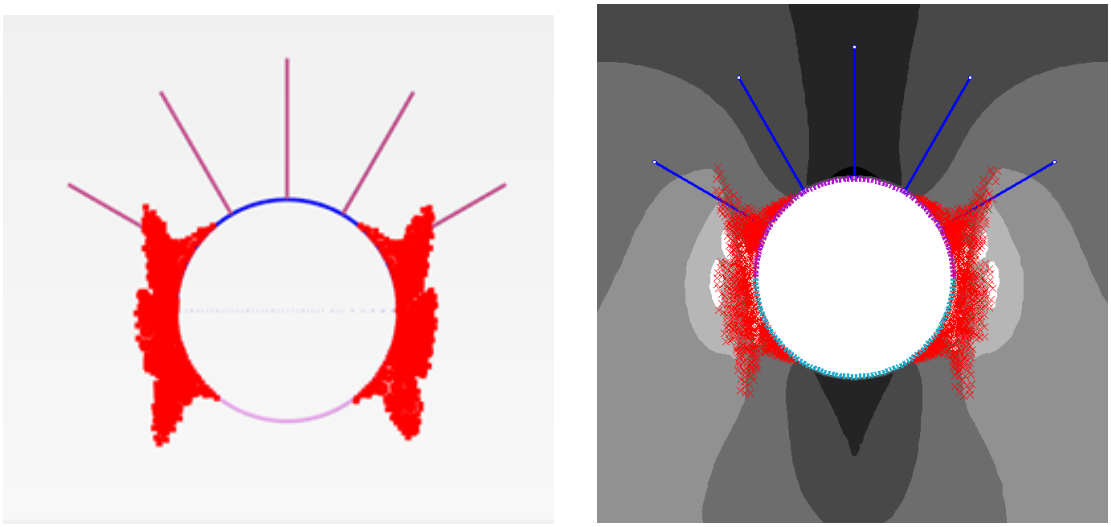

Figure 34: Plastic points in PLAXIS (left) vs. *Phase*^{2} (right) at the end stage

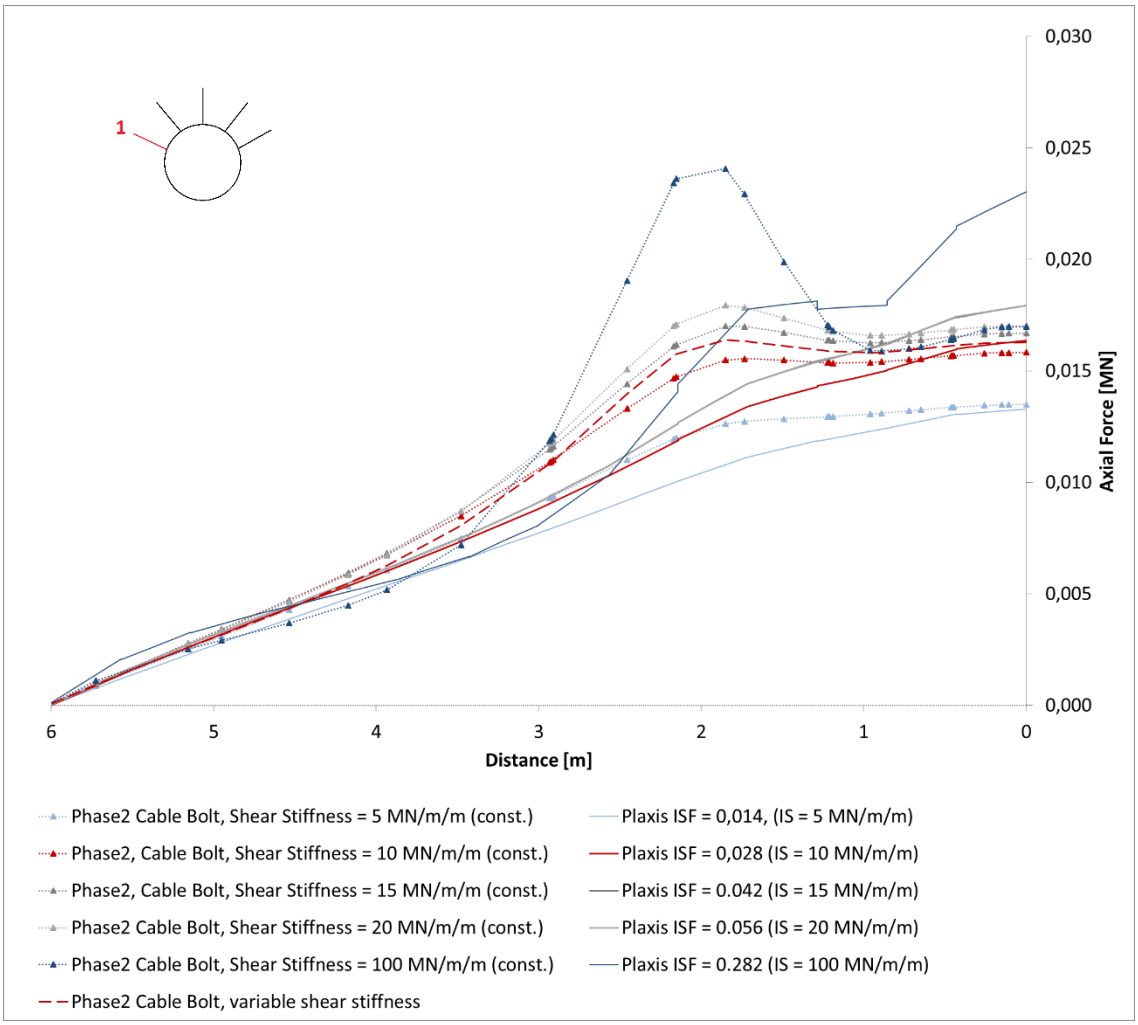

Figure 35: Anchor force 1 for varying interface shear stiffnesses

It seems like *Phase*^{2} is able to facilitate complex failure mechasims, which as a result control the mobilization of skin friction. The relatively high shear stiffness of the interface enables eventually the load transfer to the cable, leading to higher axial forces.

Furthermore, it can be seen that the results from both codes for anchor 1 agree reasonably well for low values of constant shear stiffness (between *5* and *10 MN/m/m*). The best fit with the results with variable shear stiffness is obtained for constant shear stiffness equal to *10 MN/m/m.*

In Figure 36 the results for anchor 4 from both codes are presented. The *EBR* approach yields similiar results to *Phase*^{2}, however *EBR* tends to overestimate the axial forces at small distances to the tunnel lining.

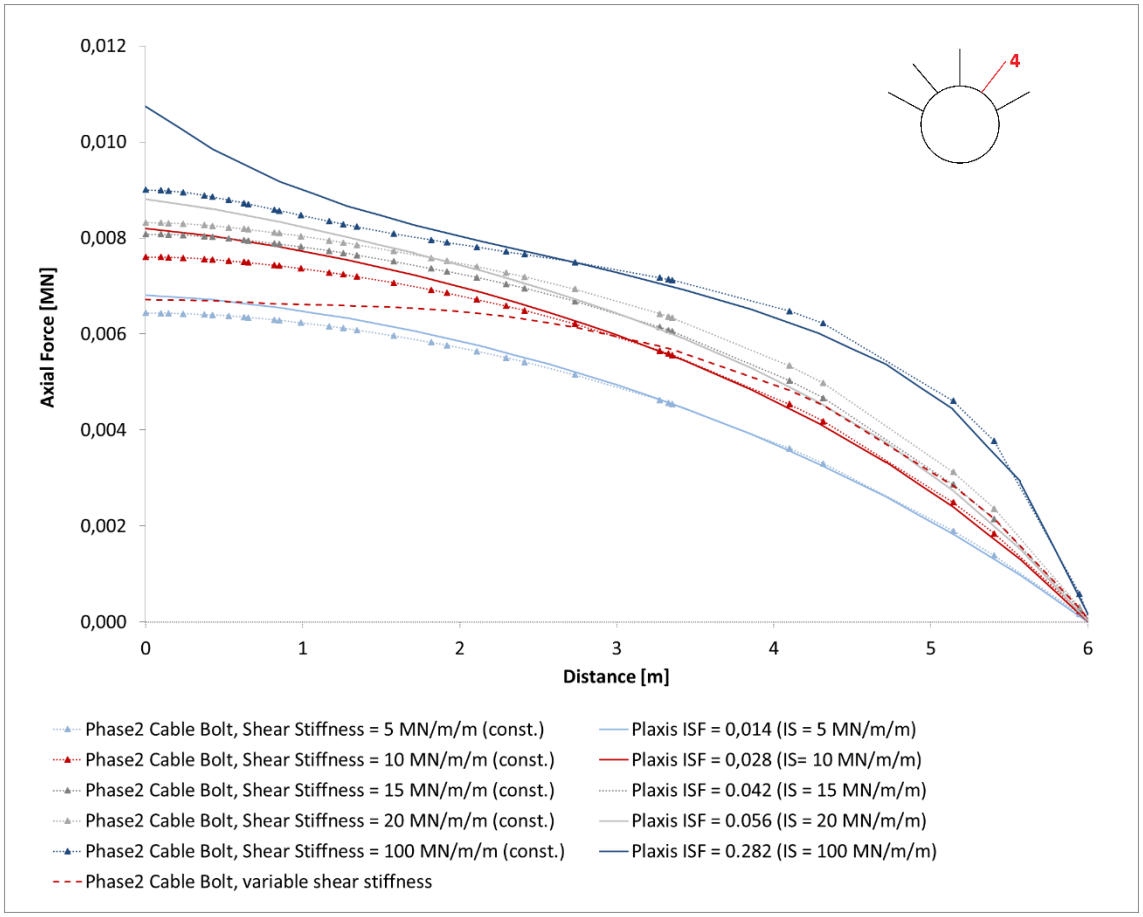

Figure 36: Anchor force 1 for varying interface shear stiffnesses

As previously mentioned, the behaviour of cable bolts is affected by various factors. In order to demonstrate the role of some of these factors, parametric analyses were performed. MC plasticity was assumed for the rock mass. For all calculations, the constant shear stiffness in *Phase*^{2} was varied in order to get the best fit to the results with variable shear stiffness. After defining the value for the constant shear stiffness, the *ISF* for the *EBR* in PLAXIS 2D were calculated and set as input parameters for the calculation in PLAXIS. Same procedure was used when changing the rock properties, stress level and cable bolt geometry. The following figures illustrate only the results obtained using the shear stiffness that yields to the best agreement between both codes. The results are compared in terms of axial force distribution along anchor 1 and anchor 4 for the last excavation stage.

5.4.1 Evaluation of the influence of rock mass properties

Influence of rock mass stiffness

To study the influence of the ground stiffness on cable bolt behaviour, the Young´s modulus of the ground was varied from *100* to *850 MPa*. Reasonable agreement between the results from PLAXIS and *Phase*^{2} were obtained for interface shear stiffness equal to *5 MN/m/m*.

The comparison of the results for the normal force along the anchors when varying the rock mass stiffness is presented in Figure 37 and Figure 38. In both codes the maximum force decreases with increasing Young´s modulus. In weak rocks the mobilized forces on the cable are higher due to the large displacements on the ground, which induce a higher force in the cable. The calculation with *Phase*^{2} delivers a plateau of almost constant force near the excavation surface, whereas *EBR* shows a nearly linear distribution of the normal force. Better agreement between both codes is achieved for relatively high rock mass stiffness, particulary in anchor 4. For weak rock conditions a significant discrepancy exists between the results in both anchors.

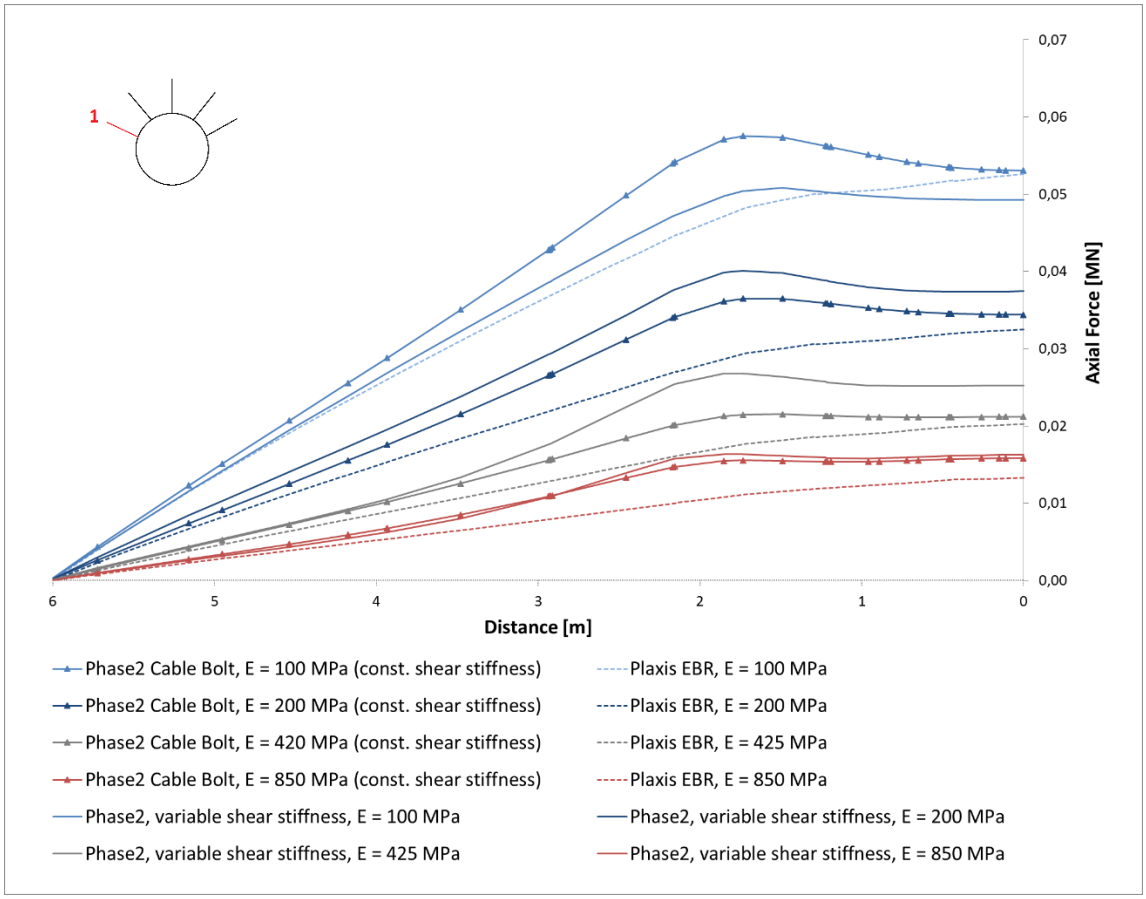

Figure 37: Anchor force 1 for varying rock mass stiffnesses (interface shear stiffness 5 MN/m/m)

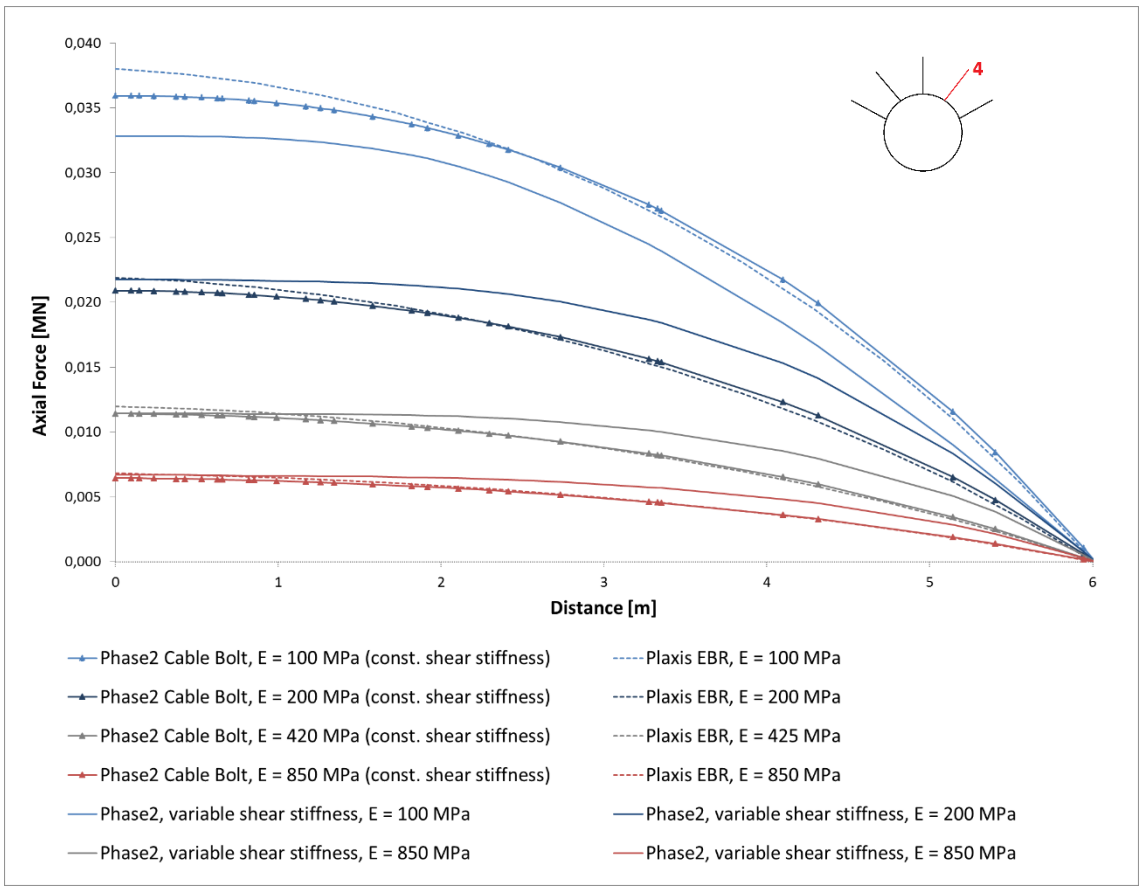

Figure 38: Anchor force 4 for varying rock mass stiffnesses (interface shear stiffness 5 MN/m/m)

Influence of rock mass strength (shear stiffness 10 MN/m/m)

The results for the *EBR* (PLAXIS) and *plain strand cable* bolts (*Phase*^{2}) are compared in Figure 39 and Figure 40. The best fit was obtained for shear stiffness of *10 MN/m/m*.

From the plots it can be seen that the results from PLAXIS reflect the trend shown in *Phase*^{2} for the normal force distribution along the bolts. As for most of the calculations presented in this study, a better agreement is achieved for anchor 4.

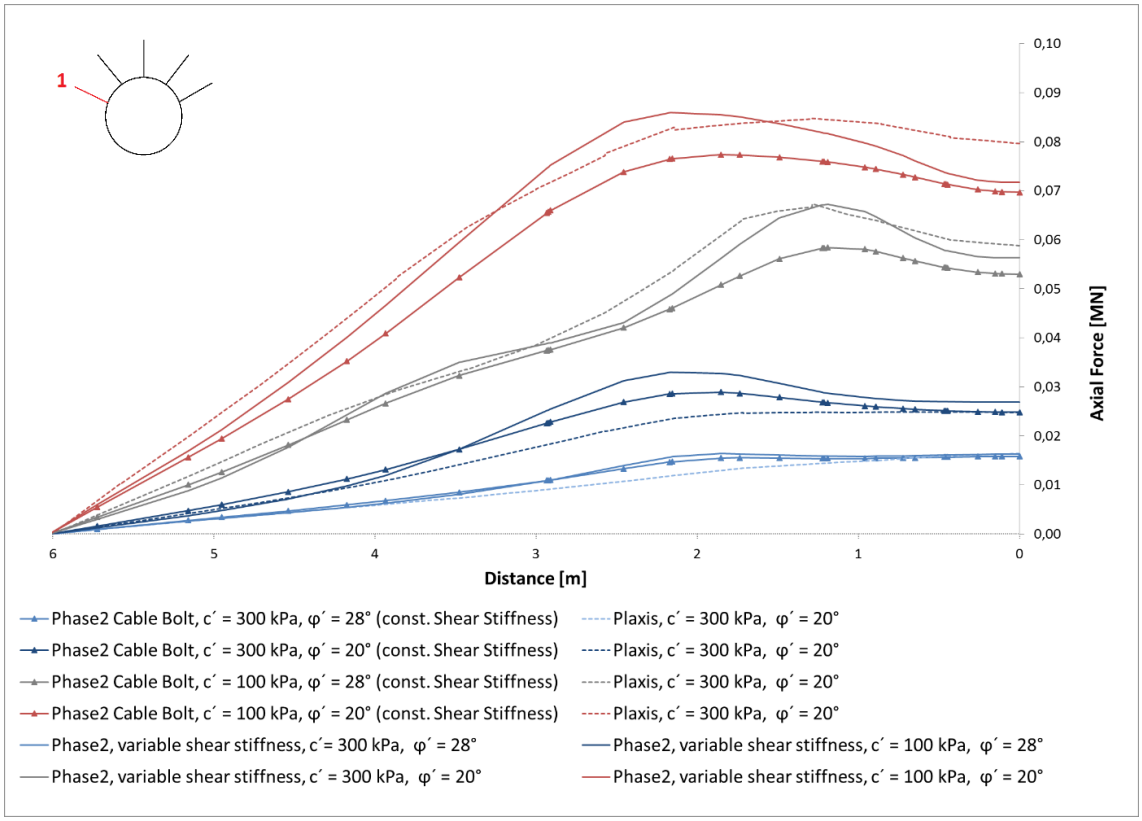

Figure 39: Anchor force 1 for varying rock mass strength (interface shear stiffness 10 MN/m/m)

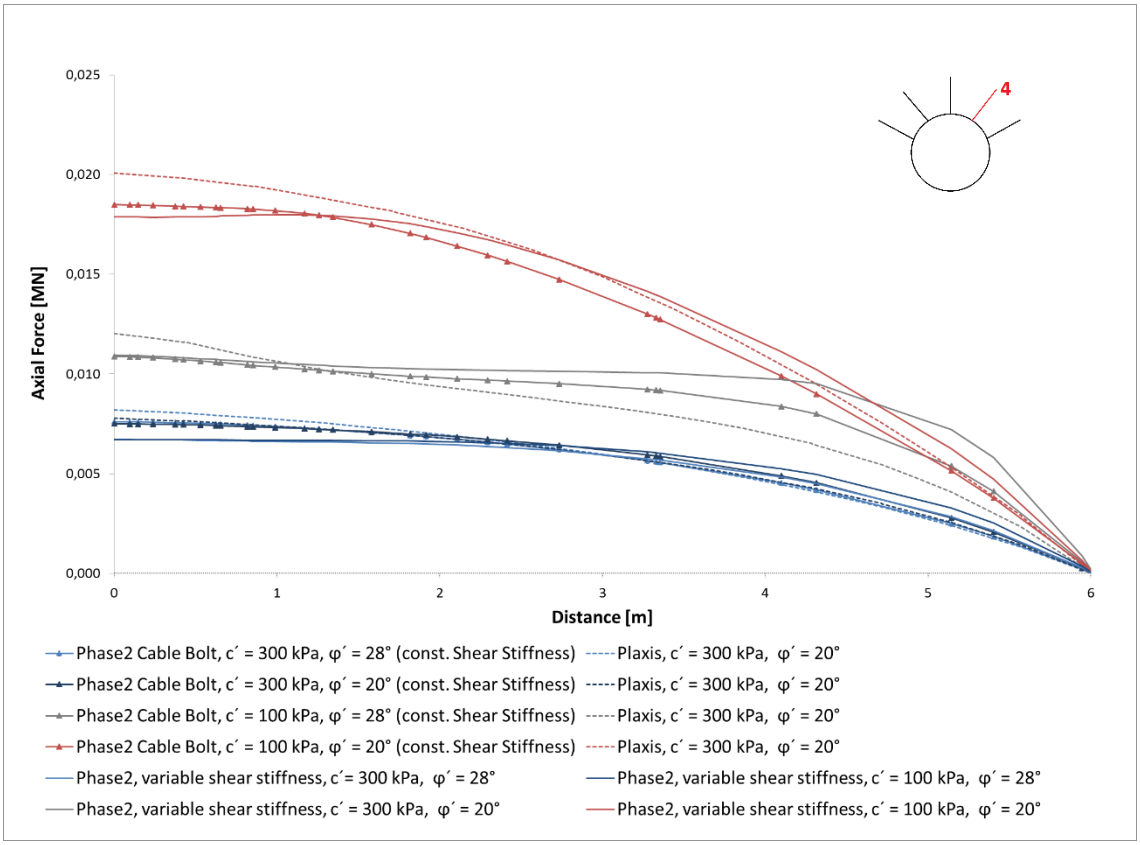

Figure 40: Anchor force 4 for varying rock mass strength (interface shear stiffness 10 MN/m/m)

5.4.2 Evaluation of the influence of stress level

To investigate the effect of the confining pressure on cable bolt behaviour, the FE-model height was varied from *50* to *100m* resulting in different stress levels in the surrounding ground. For the calculation, the shear stiffness in *Phase*^{2} was set to *10 MN/m/m*, since the best agreement between the results with constant shear stiffness from both codes and the one with variable shear stiffness in *Phase*^{2} was obtained for this value.

The results for the axial force distribution from both codes are presented in Figure 41 and Figure 42. Higher stress levels cause an increase of the forces mobilized in the anchor in both codes. Furthermore, it can be seen that the axial forces follow the same path in both codes, indicating a good performance of *EBR* in simulating the cable bolt behaviour.

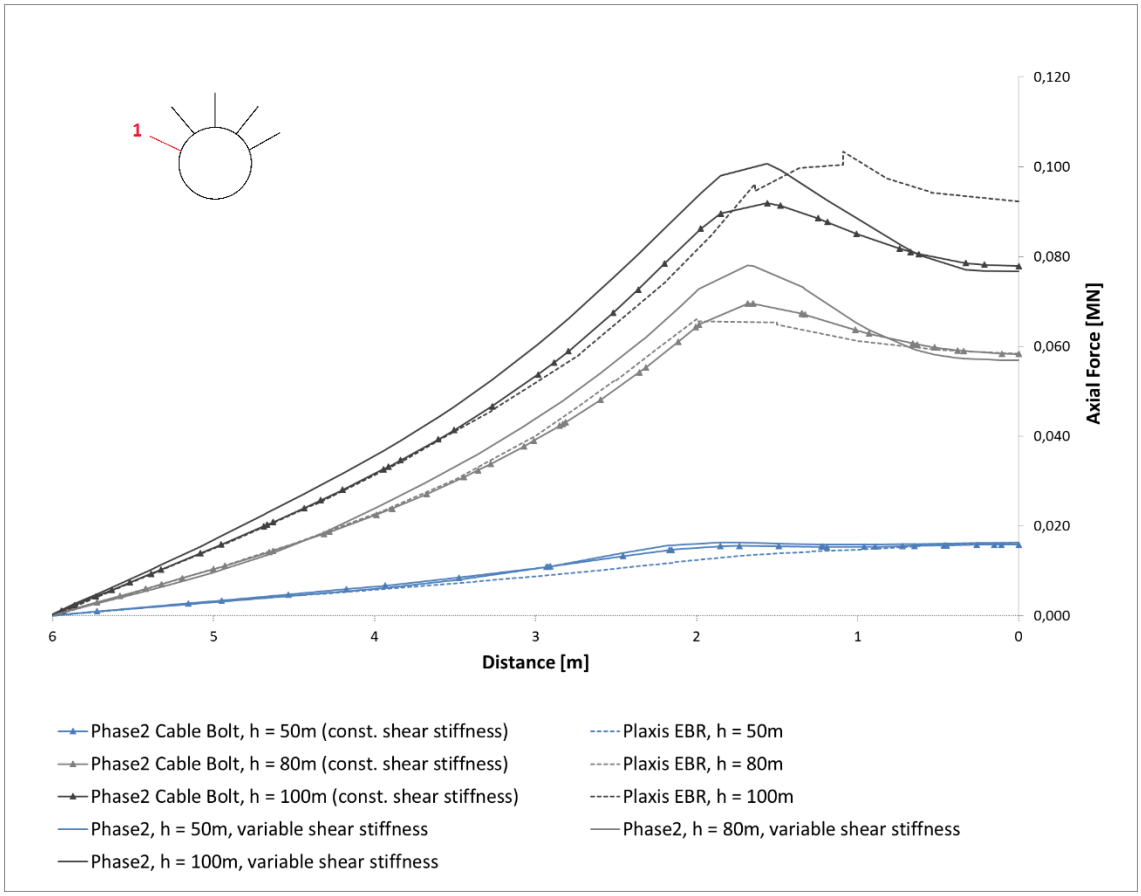

Figure 41: Anchor force 1 for varying stress levels (interface shear stiffness 10 MN/m/m)

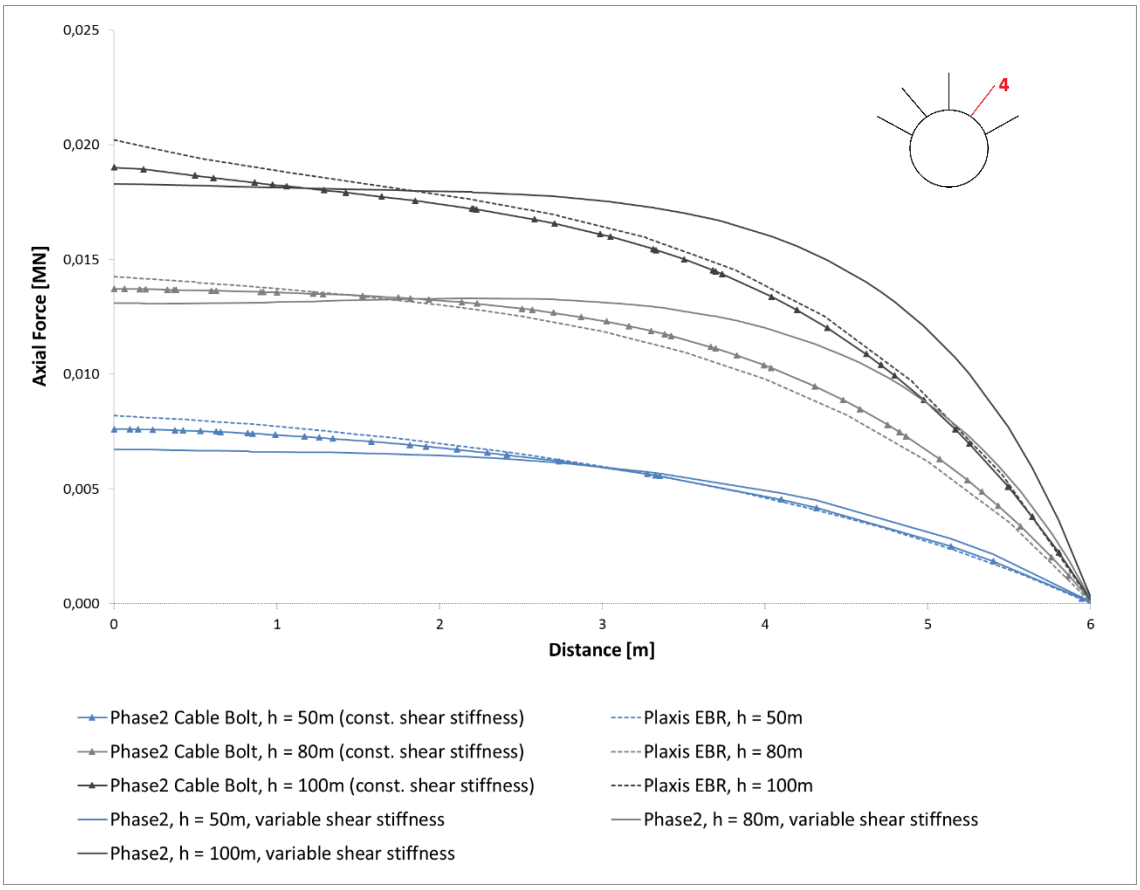

Figure 42: Anchor force 4 for varying stress levels (interface shear stiffness 10 MN/m/m)

5.4.3 Evaluation of the influence of cable bolt geometry

Influence of Borehole Diameter

The borehole diameter was varied in *Phase*^{2}, whereas in PLAXIS additionally a fictious value for the Young´s modulus of the *EBR* was defined, as explained in chapter 4.2.4. The shear stiffness was set to *5 MN/m/m*.

The comparison of the results for *EBR* in PLAXIS and *plain strand cable bolt* in *Phase*^{2} is shown in the following figures. It can be seen that the borehole diameter has no influence on the cable bolt behaviour. The agreement between both codes regarding the normal force distribution is not quite satisfactory.

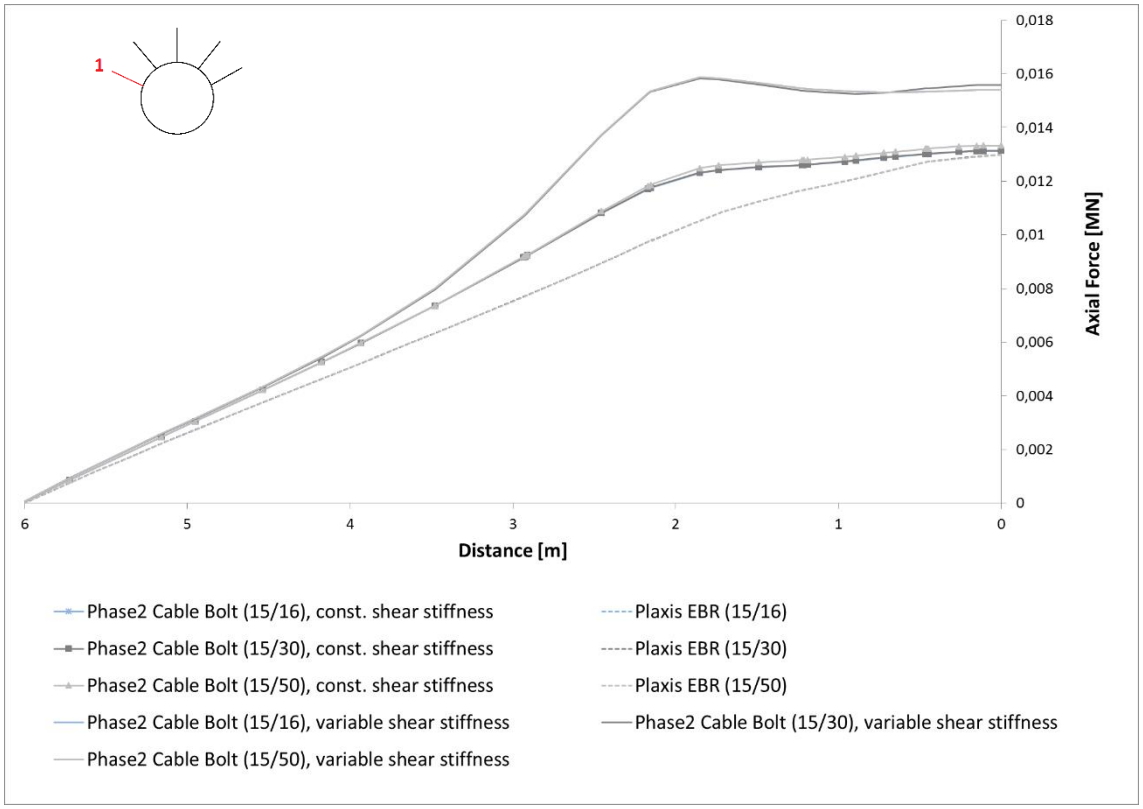

Figure 43: Anchor force 1 for 15mm cable diameter and varying borehole diameter (interface shear stiffness 5 MN/m/m)

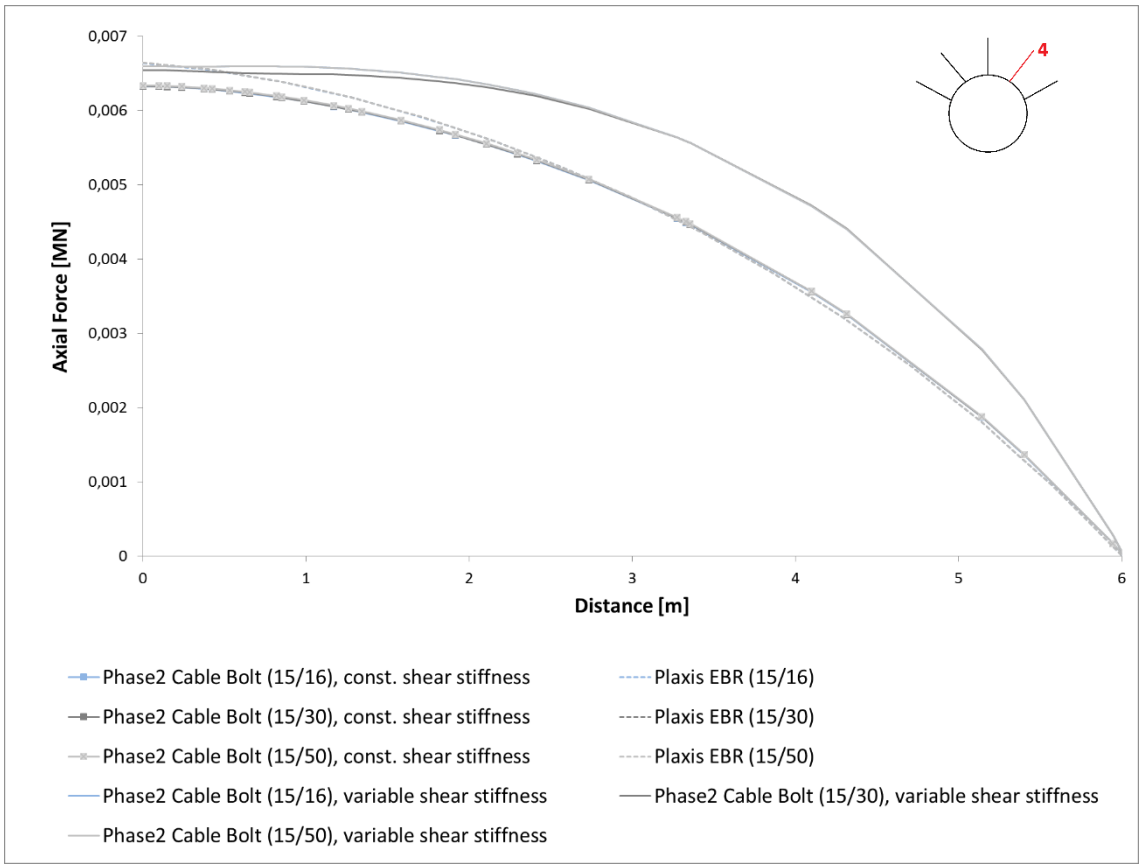

Figure 44: Anchor force 1 for 15mm cable diameter and varying borehole diameter (interface shear stiffness 5 MN/m/m)

Influence of cable diameter

Moreover the cable diameter was varied in both codes. The shear stiffness was assumed as *10 MN/m/m*. The results of the calculation are presented in the following figures. Obviously, when increasing the cable diameter a higher load can be transfered along the anchors. Furthermore, it can be seen that the maximum anchor forces are in the same range in both codes, but the behaviour is different, since a plateau of normal force near the tunnel lining is revealed in *Phase*^{2}, while the normal force in PLAXIS is almost linear.

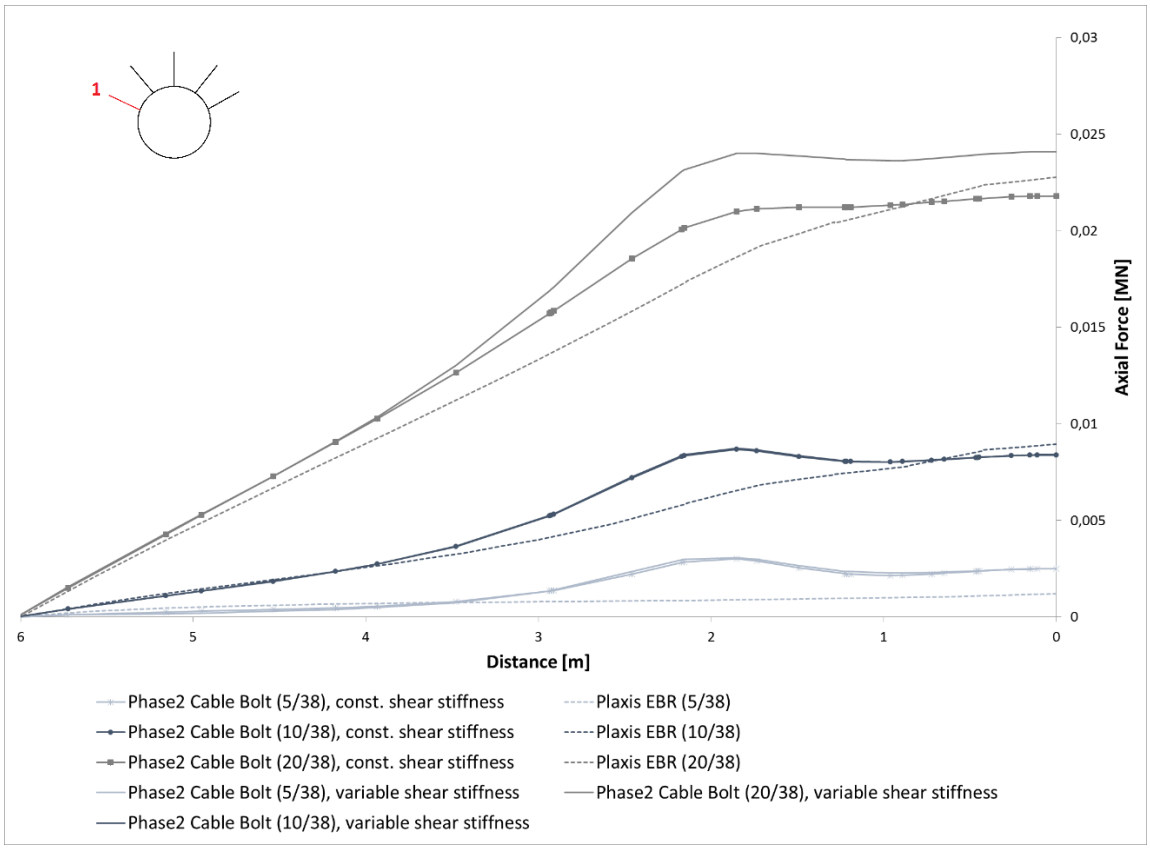

Figure 45: Anchor force 1 for varying cable diameter - borehole diameter 38mm (interface shear stiffness 10 MN/m/m)

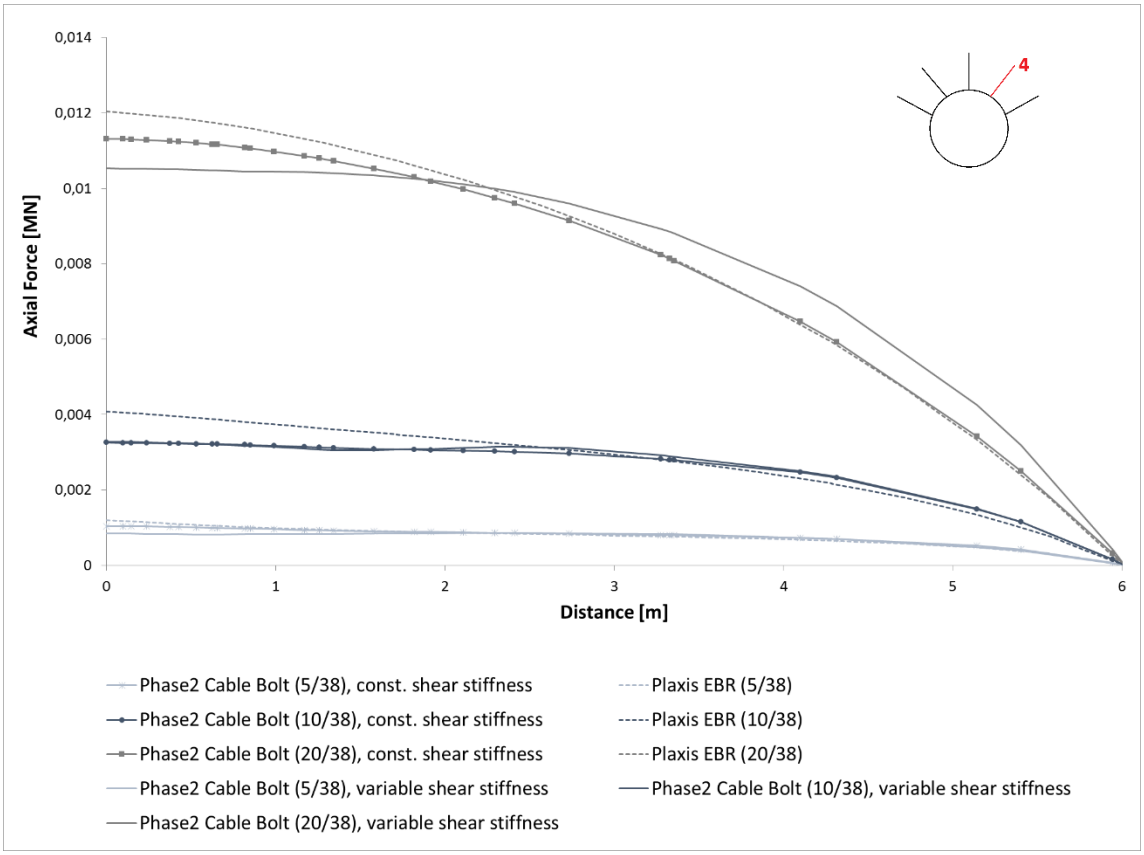

Figure 46: Anchor force 4 for varying cable diameter - borehole diameter 38mm (interface shear stiffness 10 MN/m/m)

6 Conclusion

Five different bolt models were analysed to verify the possibility of *EBR* for applications in tunneling. The following conclusions can be drawn:

Fully bonded: By artificially increasing the skin resistance, the *EBR* shows a good performance in modelling *fully bonded* bolts.

Swellex: To simulate the effect of interface slip, a low skin resistance should be defined. The validation demonstrates that *EBR* can be an effective tool for modelling *Swellex* bolts.

Tiebacks: Can be modelled as a combination of *node-to-node* anchor, which represents the anchor free length and *EBR*, which simulates the grouted part of the anchor. The results show good agreement between the two codes.

Plain strand cable bolts: The key obstacle in modelling cable bolts by means of *EBR* is the incapabilty of conseridering the effects of various factors on the shear stiffness of the cable-grout interface. Given the complex interaction between the rock mass properties, stress level and excavation geometry, it is not possible to determine *interface stiffness factors* for the *EBR* to fit every possible situation. The derived values for the *interface stiffness factors* are restricted to the cases studied in this thesis. Even though the results indicate relatively good agreement with *Phase*^{2}, one should be aware about the limitations of this model.

- At present, the interface stiffness in PLAXIS is only related to the shear modulus of the soil/rock and the out-of-plane spacing. In order to model a realistic mobilization of the skin resistance a stress-dependent interface stiffness is necessary.

- The progressive failure mechanism should also be considered and consequently the stress decrement at the interface during the debondig process.

- The formulation of *EBR* in PLAXIS is not able to capture the development of fractures in the grout. Therefore the effect of dilatancy can not be simulated (dilatancy influences the bond strength).

7 Bibliography

Algulin, J.; Pedersen, B. (2014) Modelling of a piled raft foundation as a plane strain model in PLAXIS 2D. Master thesis. Chalmers University of Technology Göteborg, Sweden

Brinkgreve, R.B.J.; Kumarswamy, S.; Swolfs, W.M. (2018a) PLAXIS 2D Reference Manual 2018. Plaxis bv. Delft, The Netherlands.

Brinkgreve, R.B.J.; Kumarswamy, S.; Swolfs, W.M. (2018b) PLAXIS 2D Material Model Manual 2018. Plaxis bv. Delft, The Netherlands.

Crotty, J.M. and Wardle, L.J. (1985) Boundary integral analysis of piecewise homogeneous media with structural discontinuities. *Int. J. of Rock Mech. And Mining Sci & Geomech. Abst.*, 22 (6), 419-427.

Cundall, P.A. (1971) A computer model for simulating progressive, large scale movements in blocky rock systems, Proc. Symp Int. Soc. Rock Mechanics, Vol. 1.

Farmer, I.W. (1975) Stress distribution along a resin grouted rock anchor, *Int. J. of Rock Mech. And Mining Sci & Geomech. Abst*., 12, 347-351.

Goodman, R.D.; Taylor, R.L.; Brekke, T.L. (1968) A model for the mechanics of jointed rock. *J. of the Soil Mech and Foundation div.*, ASCE, Vol.14, 637-659.

Hoek, E. (2007) Practical Rock Engineering

Hyett, A.J,; Bawden, W.F.; MacSporran, G.R.; Moosavi, M., (1995) A constitutive law for bond failure of fully grouted cable bolts using a modified Hoek cell, *Intl. J. Rock Mech. and Mining Sci. & Geomechanics Abstracts*, Vol 32, No.1, pp 11-36.

Hyett A.J. Moosavi M. and Bawden W.F. (1996) Load distribution along fully grouted bolts, with emphasis on cable bolt reinforcement, *Int. J. Numer and Analytical meth. In Geomech.*, 20, 517-544.

Martin L.B. (2012) Theoretical and experimental study of fully grouted rockbolts and cablebolts under axial loads. Dissertation. Ecole Nationale Superieure des Mines de Paris.

Rabcewicz, L. (1964) The New Austrian Tunnelling Method (NATM). vol. I, II, III.

Reichert, R.D.; Bawden W. F.; Hyett A. J. (1992) Evaluation of design bond strength for fully grouted cable bolts. *Bull. Can. Inst. Min. Metall*. 85, 110-118

Schädlich, B. (2013) Embedded piles for anchor modelling in PLAXIS 2D.

Sluis, J. (2012) Validation of Embedded Pile Row. Master thesis. Delft University of Technology, The Netherlands.

Stillborg, B. (1986) Professional Users Handbook for Rock Bolting (Trans Tech Publications).

Van der Kwaak, B. (2015) Modelling of dynamic pile behaviour during an earthquake using PLAXIS 2D Embedded Beam (rows). Master thesis. Delft University of Technology, The Netherlands.

Windsor, C. and Thompson A. (1993) Rock reinforcement- technology, testing, design and evaluation. Comprehensive Rock Engineering - Principles, Practice and Projects (Pergamon Press, Oxford). vol. 4. pp. 451–484.

Windsor C. and Thompson A. (1996) Terminology in rock reinforcement practice in Proceedings of the 2nd North American Rock Mechanics Symposium (Rock Mechanics: Tools and Techniques, Montreal, Canada), edited by Aubertin, Hassani & Mitri (Balkema, Rotterdam). pp. 225–232.

https://www.rocscience.com/help/rs2/pdf_files/theory/Bolt_Formulation.pdf (25.10.2018)

Appendix A

Development of the *Plain Strand Cable* model

Hyett (1994) developed a constitutive law based on a frictional-dilatational behaviour of the cable bolt bond.

To gain insight into the mechanics of load transfer between the cablebolt and the surrounding rock mass, Hyett performed a series of pull tests using a modified Hoek cell. The confining pressure at the outside of the grout annulus was mantained constant during the test. The axial displacement was increased at a rate of 0.3 mm/sec. The axial pullout force and the radial displacement were measured. To investigate the effect of the confining pressure, three or four confining pressures , which are more likely to occur at the borehole wall in operational practice, were applied. The influence of the grouting material was analyzed using three different grout qualities (w:c = 0.3, 0.4, 0.5).

The tests revealed that the bond strength increases and the radial dilatation decreases with confining pressure. The w:c cement ratio also influenced the bond strength and the radial dilatation. Stronger grout flutes (lower w:c ratio) were associated with higher bond strengths.

Three failure mechanisms may occur along the embedment length:

-dilatational slip, accomodated by radial fractures

-unscrewing of the cable from the grout

-shear failure of the bolt-grout interface

The interplay between these failure mechanisms is pressure dependent. At low pressures on the cable grout inteface, dilatational slip dominates the bond failure. At higher pressures, unscrewing or shear failure is more likely to occur. Tests showed that bond failure of cables occurs by rotation rather than shear failure (due to low torsional rigidity and helical structure), whereas for solid bolts shear failure is important. To model realistic behaviour of cable bolts, unscrewing during bond failure should be considered. In practice, all three failure modes occur concurrently. Even at high confining pressures, when no dilation occurs, the radial fractures are always present.

Hyett divided the failure process into four stages:

-Stage 1 (u_a<1 mm). The behaviour of the cabel bolt in the initial stage is controlled by the elastic properties of the cable, grout and the interface inbetween. Nevertheless, the tests results (Figure 47) indicate sensitiveness of the initial stiffness to the confining pressure. These observations confirm the frictional nature of the bond, even during the initial elastic stage.

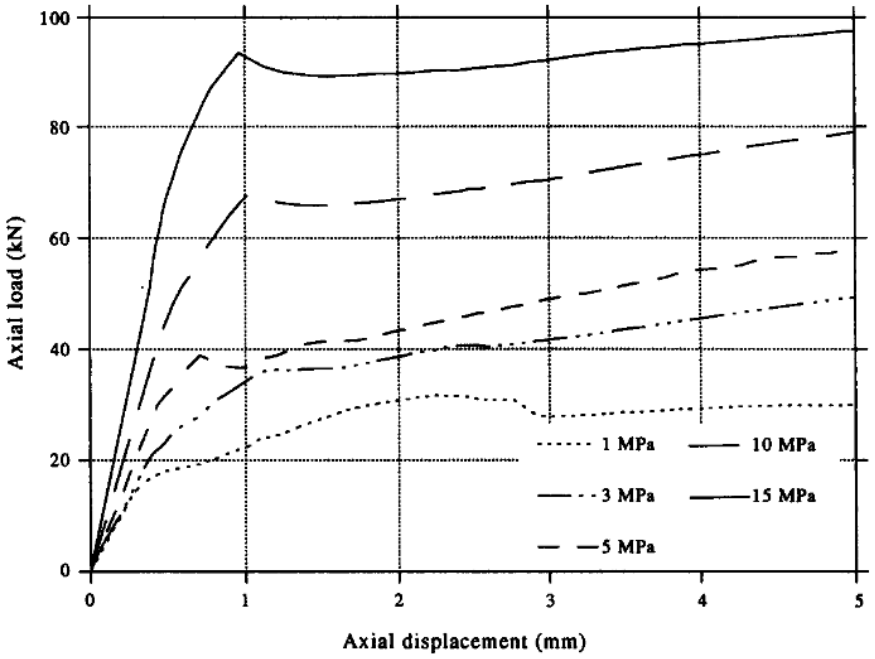

Figure 47: Axial force vs. axial displacement for 0.3 w:c ratio (Hyett et al, 1995)

Stage 2-Stage3 (splitting of the grout annulus u_a=1 mm). After 1 mm of axial displacement the cement annulus starts to split. Two mechanisms may initiate, either the individual grout wedges can be radially displaced resulting in dilatational slip, or shearing through the cement flutes. At high confining pressures the radial dilatation due to radial splitting is reversible, whereas at low confining pressure it remains.

-Stage 3 (u_a=1 – 50 mm). The most important part in the load transfer mechanism at this stage is the friction along the cable-grout interface, which prevents the cable from slipping. The failure process at the cable-bolt interface is related to the radial confinement. The frictional response is governed by the frictional properties of the cable-grout bond and the amount of stress transferred from the outer surface of the grout annulus where the pressure is applied to the cable-grout interface where slip occurs. The radial dilatation as the grout wedges are forced apart, generates extra normal pressure at the cable-bolt interface, resulting in higher bond strengths.

For cables with low torsional rigidity, unscrewing failure may occur during stage3. Less shearing and less dilatation will result in an almost perfect plastic response and lower bond strengths.

- Stage 4 (u_a>50 mm). After 40- 50mm of axial displacement, the radial dilatation is constant. The ultimate capacity is reached.

Graphical Model

Using the MHC data, and assuming the cable bolt bond failure is similiar to shear failure of rock joints, response curves have been constructed to provide insigt into the cable bolt bond behaviour (Figure 48). At low confining pressure, the cable bolt bond behaves almost perfect plastic, whereas at high pressures work hardening occurs. The friction angle at the interface can be estimated by dividing the pull force by the contact area of the interface. The radial stiffness (Quadrant 2) increases with confining pressure, as the fractures are closed.

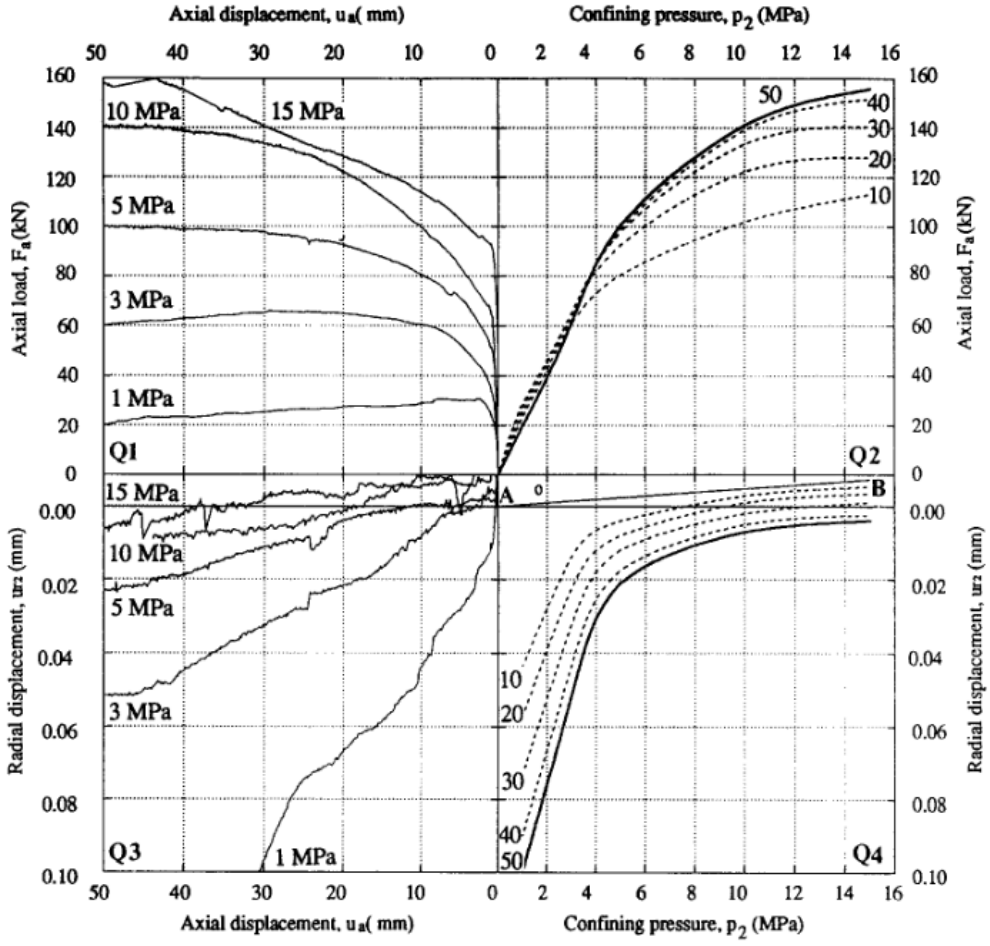

Figure 48: Cable bolt bond failure response for a 0.3 w:c, opposite the MHC results (Hyett et al, 1995)

Hyett et al. performed a series of pull tests to investigate the influence of different radial stiffnesses and variable radial pressures. Regarding the radial stiffness, higher bond strengths were observed for tests with higher radial stiffness in both experimental data and graphical model. For the tests conducted under variable

radial pressure, the graphical model couldn´t account for the path dependent effects, since the model assumes a load path independent bond strength.

Mathematical Model

The mathematical formulation makes it possible to implement the model into numerical methods.

The Cable-Grout Interface

-Splitting of the cement annulus

The radial displacement at the bolt-grout interface may be written as:

$$u_{r1} = v_0 - p_1 \quad * \frac{v_0}{(K_0 * v_0 + p_1)} - \frac{p_1}{K_{rc}} \qquad (15)$$

where v_0 represents the dilatation caused by splitting when no pressure acts on the interface ($p_1 = 0$), and K_0 the radial stiffness of the interface immediately after splitting. The third term describes the radial contraction as the pressure p_1 is applied. The radial stiffness of the cable is given by K_{rc}.

-Friction coefficients

The axial force is given by three components: the force related to dilatation slip after splitting of the grout, the force responsible for unscrewing and the force for shear failure of the grout. Since presently, no rational basis exists for the determination of the length over which shearing dominates, it is not possible to determine the exact axial force, so an average friction angle is introduced. The average axial force is then given by:

$$F_a = A_1 * p_1 * tan\phi' + Q \qquad (16)$$

where Q is the force required for untwisting of the free length of the cable and ϕ´ is the average friction angle, which can be determined experimentally.

-Dilatation angles

The relation radial displacement - axial displacement was determined empirically. Based on observations the average radial displacement along the embedment length is:

$$u_{r1} = \frac{k_1}{p_1} * (u_1 - 1) + v_0 - p_1 * \frac{v_0}{K_0 * v_0 + p_1} - \frac{p_1}{K_{rc}} \qquad (17)$$

where k1 is the empirical constant that relates the axial displacement to the radial displacements.

The Grout Annulus

The cement annulus is assumed to have fully split after 1 mm of axial displacement and no tangential loads can be transfered. Depending on the confining pressure and the dilatation at the cable-grout interface, three cases are possible.

-Case1: closed radial fractures

-Case2: partially open radial fractures

-Case3: fully open radial fractures

For the same confining pressure p_2 more stress is transfered through the grout in case 3. In this case, the incremental change in pressure at the interface depends only on the incremental change in pressure at the outer surface of the grout annulus. For cases 1 and 2, it depends also on dilatation, so even for constant p_2, p_1 increases with dilatation. The dilatation at the cable-bolt interface is in case 1 and 2 higher than at the outside of the annulus, whereas for case 3 the deformations are equal when p_2 is maintained equal.

Coupling the Grout Annulus to the Cable-Grout Interface gives the mathematical formulation to fully describe the behaviour of bond failure during a pull test. Each incremental axial displacement changes the annulus and bolt-grout interface radial response, resulting in an increment of the axial force, which is calculated.

The model also accounts for the grout quality. The use of low w:c ratio grouts (<0.40) can increase cable bolt capacities by 50% to 75% (Reichert R.D. et al, 1992). This effect is maximized under high radial confinement.

Appendix B

Input parameters for the different bolt types in *Phase²*

Table 3: Comparison of input parameters for the different bolt types in *Phase²*

			Bolt Type				
	Input parameter	Unit	End-anchored	Fully Bonded	Cable Bolt	Swellex/ Split Sets	Tieback
Bolt Properties	Bolt/Cable Diameter	*mm*	✓	✓	✓		✓
	Borehole Diameter	*mm*			✓		✓
	Bolt Modulus	*MPa*	✓	✓	✓	✓	✓
	Tensile/Peak Capacity	*MN*	✓	✓	✓	✓	✓
	Residual Tensile Capacity	*MN*	✓	✓		✓	✓
	Out-of-plane Spacing	*m*	✓	✓	✓	✓	✓
	Tributary Area	mm^2				✓	
	w:c ratio	-			✓		
	Bond Strength	*MN/m*				✓	✓
	Residual Bond Strength	*MN/m*				✓	
	Bond Shear Stiffness	*MN/m /m*					✓

			Bolt Type				
	Input parameter	Unit	End-anchored	Fully Bonded	Cable Bolt	Swellex /Split Sets	Tieback
Bolt Model	Elastic/ Plastic					✓	✓
	Joint Shear			✓	✓	✓	✓
Pre-Tensioning	Pre-Tensioning Force	*MN*	✓			✓	✓
Face Plates	Face Plates				✓	✓	✓
Add Pull-Out Force	Pull-Out Force	*MN*			✓	✓	✓
Const.Shear Stiffness	Stiffness	*MN/m/m*			✓		
Add Buldges	Bulges				✓	✓	
Bond Length	Bond Length	*% / m*					✓

Appendix C

Input parameters for the calculation PLAXIS *EBR* vs. *Phase²*

EBR (PLAXIS 2D) vs. *Fully Bonded* (*Phase²*)

Table 4: Input parameters for *EBR* (PLAXIS 2D) acc. to chapter 4.2.1

parameter		*value*	*unit*
Young´s modulus	E	210	GPa
diameter	$Ø$	0.032	m
unit weight	γ	0	kN/m^3
length	L	6	m
tensile capacity	N_p	230	kN
skin resistance start	$T_{skin,start,max}$	500	MN/m
skin resistance end	$T_{skin,end,max}$	500	MN/m
lateral skin resistance	R_s	unlimited	MN/m
base resistance	F_{max}	0	kN
axial stiffness factor	ISF_{RS}	default	-
lateral stiffness factor	ISF_{RN}	default	-
base stiffness factor	ISF_{KF}	default	-
out-of-plane spacing	$L_{spacing}$	1	m

Table 5: Input parameters for *fully bonded* bolts (*Phase²*) acc. to chapter 4.2.1

parameter		*value*	*unit*
bolt modulus	E	210	GPa
diameter	$Ø$	0.032	m
length	L	6	m

parameter		*value*	*unit*
tensile capacity	F_{yield}	0.023	MN
residual tensile capacity	F_{res}	0.023	MN
out-of-plane spacing	$L_{spacing}$	1	m

EBR (PLAXIS 2D) vs. *Swellex / Split Sets* (*Phase*^{2})

Table 6: Input parameters for *EBR* (PLAXIS 2D) acc. to chapter 4.2.2

parameter		*value*	*unit*
Young´s modulus	E	210	GPa
diameter	$Ø$	0.032	m
unit weight	γ	0	kN/m^3
length	L	6	m
tensile capacity	N_p	230	kN
skin resistance start	$T_{skin,start,max}$	5	kN/m
skin resistance end	$T_{skin,end,max}$	5	kN/m
lateral skin resistance	R_s	unlimited	kN/m
base resistance	F_{max}	0	kN
axial stiffness factor	ISF_{RS}	default	-
lateral stiffness factor	ISF_{RN}	default	-
base stiffness factor	ISF_{KF}	default	-
out-of-plane spacing	$L_{spacing}$	1	m

Table 7: Input parameters for *Swellex* bolts (*Phase²*) acc. to chapter 4.2.2

parameter		*value*	*unit*
bolt modulus	E	210	GPa
tributary area	A	804.25	mm^2
length	L	6	m
tensile capacity	F_{yield}	0.023	MN
residual tensile capacity	F_{res}	0.023	MN
bond strength		0.005	MN/m
residual bond strength		0.005	MN/m
bond shear stiffness		100	MN/m/m
out-of-plane spacing	$L_{spacing}$	1	m

EBR (PLAXIS 2D) vs. *Tiebacks* (*Phase²*)

Table 8: Input parameters for *EBR* (PLAXIS 2D) acc. to chapter 4.2.3

parameter		*value*	*unit*
Young´s modulus	E	210	GPa
diameter	$Ø$	0.032	m
unit weight	γ	0	kN/m^3
length	L	4	m
tensile capacity	N_p	230	kN
skin resistance start	$T_{skin,start,max}$	500	kN/m
skin resistance end	$T_{skin,end,max}$	500	kN/m
lateral skin resistance	R_s	unlimited	kN/m
base resistance	F_{max}	0	kN

parameter		*value*	*unit*
axial stiffness factor	ISF_{RS}	default	-
lateral stiffness factor	ISF_{RN}	default	-
base stiffness factor	ISF_{KF}	default	-
out-of-plane spacing	$L_{spacing}$	1	m

Table 9: Input parameters for *node-to-node anchor* (PLAXIS 2D) acc. to chapter 4.2.3

parameter		*value*	*unit*
Axial Stiffness	EA	169e3	kN
length	L	6	m
out-of-plane spacing	$L_{spacing}$	1	m

Table 10: Input parameters for *Tiebacks* (*Phase*^{2}) acc. to chapter 4.2.3

parameter		*value*	*unit*
bolt diameter	$Ø$	0.032	m
borehole diameter	$Ø$	0.034	m
bolt modulus	E	210	GPa
length	L	6	m
bond length	L_{bond}	4	m
tensile capacity	F_{yield}	0.023	MN
residual tensile capacity	F_{res}	0.023	MN
bond strength		5	MN/m
bond shear stiffness		100	MN/m/m
out-of-plane spacing	$L_{spacing}$	1	m

EBR (PLAXIS 2D) vs. *Plain Strand Cable Bolt* (*Phase*^{2})

Table 11: Input parameters for *EBR* (PLAXIS 2D)

parameter		*value*	*unit*
Young´s modulus	E	34	GPa
diameter	$Ø$	0.038	m
unit weight	γ	0	kN/m^3
length	L	6	m
tensile capacity	N_p	230	kN
skin resistance start	$T_{skin,start,max}$	500	kN/m
skin resistance end	$T_{skin,end,max}$	500	kN/m
lateral skin resistance	R_s	unlimited	kN/m
base resistance	F_{max}	0	kN
axial stiffness factor	ISF_{RS}	0.028	-
lateral stiffness factor	ISF_{RN}	0.028	-
base stiffness factor	ISF_{KF}	1	-
out-of-plane spacing	$L_{spacing}$	1	m

Table 12: Input parameters for *Plain Strand Cable Bolts* (*Phase*^{2})

parameter		*value*	*unit*
cable diameter	$Ø$	15.2	mm
borehole diameter	$Ø$	38	mm
cable modulus	E	210	GPa
length	L	6	m
cable peak		0.023	MN
water cement ratio	$w:c$	0.35	-
out-of-plane spacing	$L_{spacing}$	1	m

Appendix D

Modelling of *End Anchored* bolts

Node-to-node anchors are used in PLAXIS in order to simulate the behaviour of *end-anchored* bolts. The necessary parameters for modelling of anchors in both codes are given in Table2. Mohr Coulomb plasticity is assumed for the rock mass. The results from the calculation with PLAXIS and *Phase²* are presented in the following figures. Both codes deliver constant normal force distribution, since these bolts are connected to the structural elements only through the endpoints and there is no interaction with the surrounding ground. Some differences between the results from PLAXIS and *Phase²* are notable in the axial force for anchor 1 (Figure 49). The difference may be related to the different discretization of the tunnel lining in both codes, that results in slightly different displacements of the connection point of the anchor to the lining. However, for anchor 4 the results are in good agreement (Figure 50).

Table 13: Input parameters for *node-to-node anchor* (PLAXIS 2D)

parameter		*value*	*unit*
Axial Stiffness	EA	169e3	kN
length	L	6	m
out-of-plane spacing	$L_{spacing}$	1	m

Table 14: Input parameters for *End Anchored* bolts (*Phase²*)

parameter		*value*	*unit*
bolt diameter	$Ø$	32	mm
bolt modulus	E	210000	MPa
length	L	6	m
tensile capacity	F_{yield}	0.023	MN
residual tensile capacity	F_{res}	0	MN
out-of-plane spacing	$L_{spacing}$	1	m

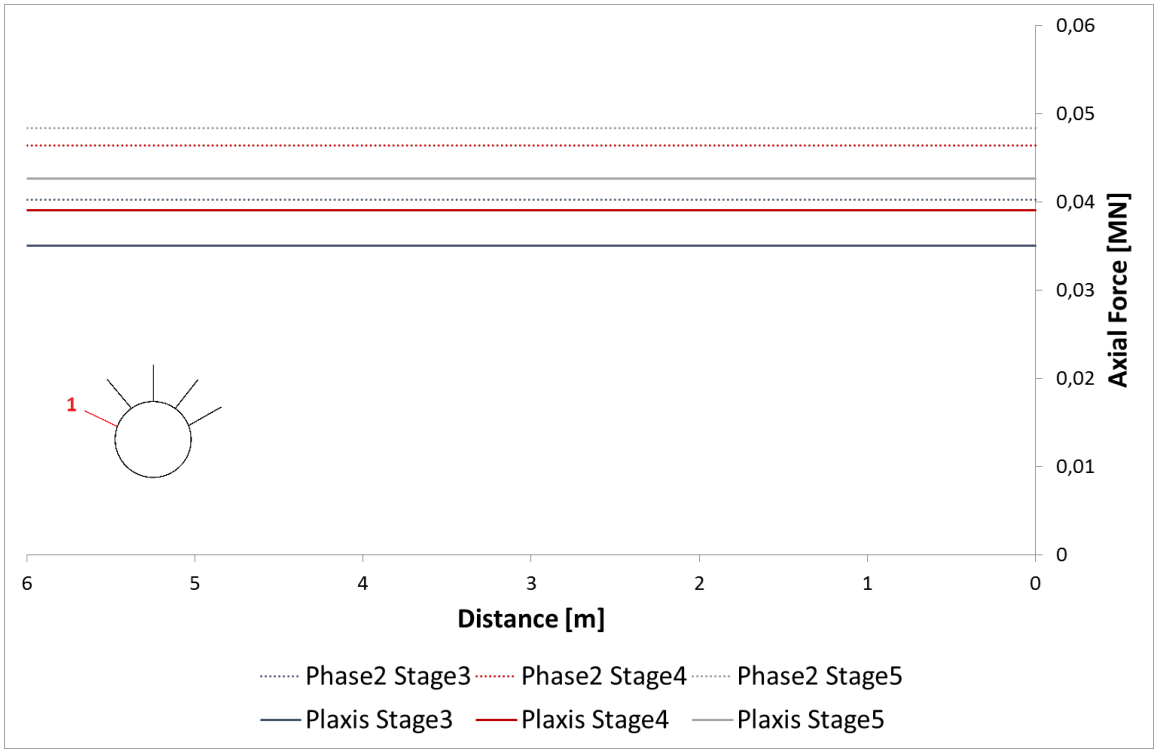

Figure 49: Axial force in anchor 1 for MC rock and node-to-node anchor (PLAXIS) vs. end anchored bolts (*Phase*^{2})

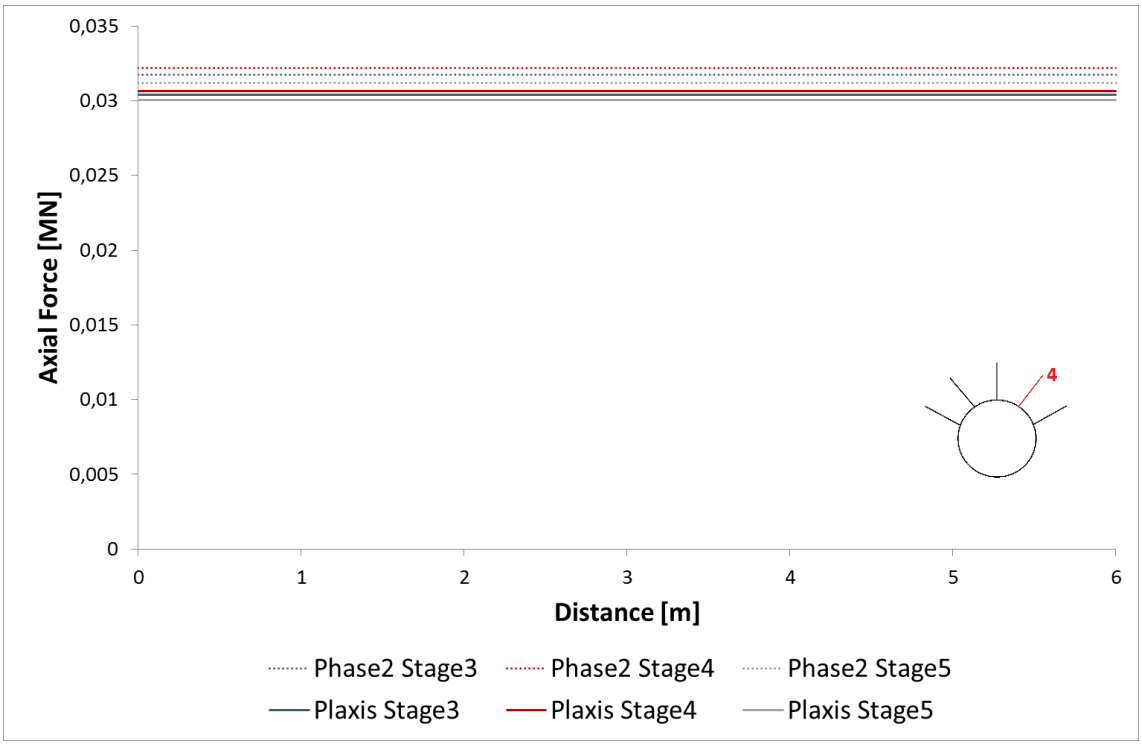

Figure 50: Axial force in anchor 1 for MC rock and node-to-node anchor (PLAXIS) vs. end anchored bolts (*Phase*^{2})